# Synthetic lethal screening identifies existing drugs with selective viability effects on Neurofibromatosis type-1 model systems

Wang, Y.[1,2,†], Stevens, M.[1,3,†], Mandigo, T.R.[4], Bouley, S.J.[4], Sharma, A.[4], Sengupta, S.[1,3], Housden, A.[1], Perrimon, N.[5,6], Walker, J.A.[4,7*], Housden, B.E.[1,3,*]

[1] The Living Systems Institute, University of Exeter, Exeter, UK

[2] The First People's Hospital of Qinzhou, China

[3] The College of Medicine and Health, University of Exeter, Exeter, UK

[4] Center for Genomic Medicine, Massachusetts General Hospital, Boston, MA 02114, USA

[5] Department of Genetics, Blavatnik Institute, Harvard Medical School, Boston, MA, 02115, USA

[6] Howard Hughes Medical Institute

[7] Cancer Program, Broad Institute of MIT and Harvard, Cambridge, MA 02142, USA

[†] These authors contributed equally

* Correspondence to b.housden@exeter.ac.uk and jwalker@helix.mgh.harvard.edu

## ABSTRACT

Neurofibromatosis type 1 (NF1) is a genetic multi-system disorder. Symptoms include near universal benign neurofibromas, as well as malignant tumours, including generally fatal malignant peripheral nerve sheath tumours. There are limited therapies for any NF1-associated tumours; therefore, there is a clear clinical need to discover new drugs that specifically target NF1-deficient tumour cells. Using a *Drosophila* NF1-KO cell model, we used synthetic lethal screening to identify candidate drug targets for NF1-deficient tumours and performed statistical enrichment analysis to identify further targets. We then assessed the top 72 candidate synthetic lethal partner genes to *NF1* using Variable Dose Analysis, resulting in 15 candidate genes that decreased NF1-KO viability by >10% and were novel druggable targets for NF1. Autophagy inhibitors Chloroquine (CQ) and Bafilomycin A1 resulted in a significant reduction in NF1-KO cell viability, which was conserved in a panel of human NF1 mutant cell lines. AZT and Enzalutamide also selectively reduced NF1 mutant cell viability in human cell lines. Furthermore, the effect of CQ was conserved in a *Drosophila NF1*-mutant *in vivo* model. This study highlights two key points: 1) The use of *Drosophila* cells as a model to screen for drugs specifically targeting NF1 mutant cells was highly successful as candidate interactions were conserved across a panel of human NF1 mutant cells and an *in vivo* fly *NF1* mutant model, and 2) NF1-deficient cells have vulnerability to disruption of the autophagy pathway, telomerase activity, and AR activity. These pathways/drugs represent promising targets for the potential treatment of NF1-associated tumours.

**Key Words**

Neurofibromatosis type 1; Synthetic lethality; Drug repurposing; Drosophila; Autophagy

## INTRODUCTION

Neurofibromatosis type 1 (NF1) (LAWRENCE *et al.* 2014), is a genetic disorder with autosomal-dominant inheritance affecting 1 in ~3,000 (EVANS *et al.* 2010). Although the penetrance of NF1 is virtually complete after childhood, the disease is characterized by highly variable clinical expressivity. Symptoms include near universal benign, but often disfiguring, peripheral nerve associated tumours known as neurofibromas, as well as malignant tumours, including usually fatal malignant peripheral nerve sheath tumours (MPNSTs). While the tumour suppressor role of NF1 has received much attention, NF1 is a multi-system disorder where non-tumour symptoms contribute significantly to its morbidity. These non-tumour symptoms include skeletal and vascular abnormalities, pigmentation defects, reduced overall growth, and cognitive deficits, the latter seen in 50-70% of children with NF1 (GUTMANN *et al.* 2017). In part reflecting higher rates of vascular defects and cancer, the life expectancy of NF1 patients is reduced by 15-20 years (RASMUSSEN *et al.* 2001).

NF1 is caused by loss of neurofibromin, a 320 kDa protein whose only widely accepted function is to serve as a Ras GTPase Activating Protein (RasGAP) for H-, K-, N-Ras and R-Ras1, 2 and 3 (MARTIN *et al.* 1990). RasGAPs promote the conversion of active Ras-GTP into inactive Ras-GDP by stimulating the low intrinsic rate of Ras-GTP hydrolysis (SIMANSHU *et al.* 2017). Consequently, loss of neurofibromin can result in misregulation of signalling downstream of Ras, the best documented being the RAF/MEK/ERK and PI3K/AKT/mTOR pathways. Although dysregulated Ras signalling is believed to be the proximal cause of NF1 symptoms, it is unclear which of the numerous effectors downstream of Ras are relevant for disease progression, as well as the identities of the disease-pertinent targets of the signalling pathways mediating their effects. The situation is further complicated since there is undoubtedly crosstalk between these different pathways. In patients with *NF1*-driven malignant tumours, targeting Ras pathway components such as MEK or ERK is a reasonable therapeutic option, although Ras is subject to highly robust regulation (SIMANSHU *et al.* 2017), which may explain why, despite considerable effort, no effective therapy for Ras-driven cancers has yet emerged. However, chronically blocking Ras may never be an appropriate strategy for treating the many serious but non-life-threatening symptoms of NF1, especially in children.

Currently, there are limited therapies for any NF1-associated tumours. The only available drug is the MEK inhibitor Selumetinib, which was approved for use in a subset of paediatric plexiform neurofibromas in April 2020. However, not all tumours were responsive to treatment and serious side effects can be associated with Selumetinib use (GROSS *et al.* 2020; BALDO

*et al.* 2021). Therefore, there is a clear clinical need to discover new drugs that specifically target NF1-deficient tumour cells either alone or in combination.

One approach to identify candidate drug targets for tumorigenic diseases is to use synthetic lethal interaction screens. Synthetic lethal interactions are a type of genetic interaction in which inhibition of either of two genes alone is viable, but the combined inhibition of both genes is inviable. When one of these genes is mutated in tumour cells, such interactions can be exploited to kill those cells exclusively by targeting the synthetic lethal partner gene using a drug (KAELIN 2005). This approach is attractive because treatment is expected to be lethal to tumour cells but have no effect on wild-type, healthy cells.

Despite long-term interest in the use of synthetic lethality as a therapeutic strategy to treat tumours, few drugs have successfully progressed to clinical use. One example are PARP inhibitors, which exploit a synthetic lethal interaction between the DNA damage repair pathway and *BRCA1/2*, which are often mutated in breast and ovarian cancers (LORD AND ASHWORTH 2017). However, a major factor preventing successful development of treatments against synthetic lethal interactions is a lack of consistency between interactions identified in different genetic backgrounds (RYAN *et al.* 2018). This results in a lack of translation of candidate targets between model systems. Our approach to overcome this limitation makes use of *Drosophila* cells to initially identify synthetic lethal interactions with genes mutated in tumours. The reduced redundancy between gene functions in *Drosophila* permits the identification of interactions using RNA interference (RNAi) that may be otherwise hidden in human cells. The conservation of candidate interactions can then be assessed in a range of other model systems including human cells, providing a filter to remove interactions that are specific to *Drosophila*. This approach has previously proved successful, leading to the discovery of mizoribine and palbociclib as promising candidates for the treatment of tuberous sclerosis complex (TSC) and VHL-linked cancers respectively (HOUSDEN *et al.* 2015; VALVEZAN *et al.* 2017; NICHOLSON *et al.* 2019). In both cases, hits from *Drosophila* synthetic lethal screens were validated with a high success rate in both human cells and mouse models.

Given the previous success of using the *Drosophila* approach, we have applied this method to identify candidate drug targets to treat NF1-deficient tumours. Here, we describe the generation of a NF1 null mutant *Drosophila* cell line using CRISPR and its use in synthetic lethal screens to identify candidate drug targets to specifically kill NF1-associated tumour cells. We find that inhibition of autophagy (using Chloroquine (CQ) and Bafilomycin A1) has a selective effect on both a NF1-deficient *Drosophila* cell line and in an *in vivo* fly model. Furthermore, we show that this selective effect is conserved in multiple human tumour-derived

cell lines. In addition, we identify selective effects with Azidothymidine (AZT) and Enzalutamide, indicating that these repurposed drugs may have promise for the treatment of NF1 tumours in the future.

## RESULTS

### Generation of a *Drosophila* NF1 cell model cell using CRISPR/Cas9 gene editing

Our previous studies have demonstrated the potential of using cross-species genetic screens to identify candidate therapeutic targets for human disease (HOUSDEN *et al.* 2015; HOUSDEN *et al.* 2017b; NICHOLSON *et al.* 2019). The NF1 gene is well conserved between *Drosophila* and humans with 68% identity at the amino acid level (**Fig. S1**). To use the same approach to find new targets for the treatment of NF1 tumours, we first used CRISPR gene editing to generate mutations in NF1 in a *Drosophila* cell line. S2R+ cells were transfected with Cas9 and sgRNA designed to target a double-strand break in exon 2 of NF1 (**Fig. 1A**). Briefly, transfected cells expressing high levels of CRISPR reagents were isolated using FACS and single-cell cloned, as described in detail previously (HOUSDEN *et al.* 2015; HOUSDEN *et al.* 2017c). Clones were assessed using high-resolution melting analysis (HRMA) to identify those carrying mutations at the target locus. Finally, sequencing was used to confirm that induced mutations were homozygous and resulted in frameshifts in NF1 (**Fig. 1A**). Of note, S2R+ cells are aneuploid (LEE *et al.* 2014) and we found that they have three copies of the NF1 gene.

The resulting NF1-KO S2R+ cell line (hereafter called NF1-KO) was characterized by assessing the expression of neurofibromin using western blots. We found no detectable signal in the NF1-KO line when compared to parental WT S2R+ cells (**Fig. 1B**). Given that neurofibromin is a negative regulator of Ras, we assessed the growth and proliferative phenotypes of NF1-KO cells compared to WT cells. Consistent with deregulation of a mitogenic pathway, NF1-KO cells showed an increased rate of growth as measured using CellTiter-Glo assays to assess total ATP levels in the population. This effect was observed in the absence of serum in the culture media and in the presence of serum (**Fig. 1C**), indicating that culture growth is both accelerated in the absence of NF1 and is decoupled from upstream growth factor signalling pathways. To determine whether this increase in culture growth was due to increased proliferation, increased cell growth or both, we performed cell counts following culture in full serum and CellTiter-Glo assays on normalised numbers of cells from each genotype (baseline readings). Cell counts for NF1-KO showed an increase in cell numbers following culture compared to WT cells and the 'baseline' CellTiter-Glo showed no difference (**Fig. 1C**). This suggests that the difference in culture growth is primarily due to increased cell proliferation rather than an increase in cell size or ATP content of the cells.

Together, these results indicate that the NF1-KO line represents a novel NF1 null mutant cell model, with properties consistent with known effects of NF1 loss.

**Mapping synthetic lethal interactions in *NF1*-deficient *Drosophila* cells using a genome-wide RNAi screen**

We used our *Drosophila* NF1-deficient cell line to screen for synthetic lethal interactions. We used a genome-wide dsRNA library to screen in both WT and NF1-KO cells (**Fig. 2A**). Screens were performed in triplicate to allow identification of reproducible results. First, we normalised results to the median of each row and column to remove position effects and scale results from all assay plates to allow direct comparison (see methods for details). Z-scores were then calculated for each dsRNA reagent for each replicate screen and correlation between replicates was used to assess the quality of screen results. We note that some assay plates were affected by position effects. These were identified manually and removed from the analysis prior to correlation analysis. Correlation coefficients ranged between 0.9 and 0.99 (average 0.93) for control wells and between 0.55 and 0.66 (average 0.61) for non-control wells (**Fig. 2B-C**), illustrating a high rate of reproducibility between replicates. Next, we identified synthetic lethal interactions by filtering the results for dsRNA reagents that reduce the viability of NF1 cells (median $Z<-1.5$) to a greater extent than wild-type cells (median $Z\geq-1.5$). This analysis identified 134 candidate genes (**Table S1**).

Genetic screens are often associated with false-positive results due to off-targets from dsRNA reagents or noise in the screen assay. To remove potential false positives, we overlaid the screen hits onto a protein-protein interaction network from the String database (SZKLARCZYK *et al.* 2019). Synthetic lethal interactions are generally similar between genes that have related functions. Therefore, proteins that physically interact might be expected to share synthetic lethal interactions. Using the combination of physical and genetic interaction data, we can therefore remove false positives from the screen results by isolating only hits that have physical interactions with at least one other hit from the genetic interaction screen. In addition, we filtered the candidates to isolate only those with clear orthologs in humans. Following this process, 54 high-confidence candidate targets remained, 46 of which were conserved in humans (**Fig. 2D, Table S2**).

**Statistical enrichment analysis of candidate drug targets**

We used a range of methods to perform statistical enrichment analysis of the 54 candidate genes, including GO-term enrichment and semantic similarity analysis, KEGG pathway enrichment, and further protein-protein interaction mapping. A flow diagram to show the process of enrichment analysis in shown in **Fig. 3A**.

*GO enrichment and semantic similarity analysis*

During the first stage of analysis, we identified GO terms that were significantly represented by the 54 candidate gene terms (FDR < 0.05). This resulted in 215 enriched terms in biological processes (BP), 43 enriched terms in molecular function (MF), and 79 enriched terms in cellular component (CC) subcategories (**Table S3a)**. Semantic similarity between terms was visualised using the Revigo tool (http://revigo.irb.hr/), with an example shown in **Fig. 3B** for MF; semantic similarity was observed between "*histone methyltransferase activity (H3-K4 specific)"* and *"N-methyltransferase activity"*. As the candidate genes are synthetic lethal partner genes to NF1, we further performed semantic similarity analysis of candidate gene GO terms with *NF1* GO enriched terms (BP: 53 terms, MF: 5 terms, and CC: 9 terms) (**Table S3b**). GOSemSim package in R (YU 2020) was used to assign a semantic contribution factor between 0 and 1, where >0.8 indicates "in a relationship" and 0.6-0.8 indicates "part of a relationship". Genes included in terms identified to have semantic similarity were screened for those that could be targeted by FDA-approved drugs, resulting in the addition of RAC1, EGFR, FGFR, EZH2, and hTERT.

*KEGG pathway analysis*

KEGG pathway enrichment analysis identified 15 pathways associated with the candidate gene list (including the three examples shown in **Fig. 3C**: proteosome, ubiquitin-mediated proteolysis, and oxidative phosphorylation). In addition, there were two pathways that were common to the candidate genes and *NF1*: MAPK signalling pathway and EGFR tyrosine kinase inhibitor resistance pathway. These pathways were used to screen for additional genes located upstream/downstream of the candidate gene signalling pathways that could be targeted with FDA-approved drugs. This resulted in the identification of MYC, AR, CUL1, and mTOR.

*Protein-protein interaction analysis*

Finally, we assessed protein-protein interactions of the individual genes in the screen using the String database (https://string-db.org/) (SZKLARCZYK *et al.* 2019) to identify interactions with additional genes that could be targeted with FDA-approved drugs. Some examples include the interaction of SHF (candidate gene) with PDGFRA (FDA-approved drug target) (**Fig. 3D**) and the interaction of PEBP1 (candidate gene) with MEK, KRAS, and RAF1 (all FDA-approved drug targets). This resulted in the identification of PDGFRA, RAF1, MEK, KRAS, MT-CYB, BECN1, RP, GFAP, SKP1, USP14, SAMHD1, and CDC37.

In total, we identified 19 additional candidate human proteins that were filtered to those that could be targeted with FDA-approved drugs, 17 of which had *Drosophila* orthologs **(Table S3c)**. Therefore, from the genome-wide screen and statistical enrichment analysis, we generated a total of 73 candidate drug targets.

**Validation of candidate synthetic lethal interactions using Variable Dose Analysis (VDA)**

To assess the validity of the network, we tested seven highly ranked genes based on the difference in median Z-score between NF1-KO and wild-type cells with various biological functions using low throughput variable dose analysis (VDA) assays (HOUSDEN *et al.* 2017a) (**Table 1**). shRNAs expressing plasmids were generated targeting each of the seven genes and were transfected into WT and NF1-KO cells in combination with shRNA against *NF1* or against a negative control gene (*white*). Six of the seven reagents showed a significantly different VDA signal when combined with *NF1* shRNA **(Fig. 4A)**.

We then used the VDA assay as an additional combinatorial screen to assess synthetic lethality between *NF1* and all 72 candidate drug targets. Two shRNAs targeting each of the genes were generated. These reagents were then tested in WT and NF1-KO cells. Of the 72 genes, 59 showed a >10% reduction in viability in NF1-KO cells compared to WT controls (**Fig. 4B**; ranked in order of effect on NF1-KO viability relative to WT). These results indicate that the network is a reliable representation of the synthetic lethal interaction profile of the *NF1* gene.

In order to identify potential drugs for repurposing to treat NF1 tumours, we filtered the candidate gene list to those that could be targeted by existing drugs. This resulted in 22 candidate drugs targets (**Fig. 4C**). Dsor1 (MEK) and Ras85D (RAS) were in the top five candidate drug targets (based on difference in viability effect in NF1 and S2R+ cells using VDA assays), highlighting the validity of the screen. We then removed candidates that had previously been studied in relation to NF1, leaving 13 candidate drug targets (**Table 2**). Finally, we added an additional two candidate targets that were identified in the statistical enrichment analysis and do not have *Drosophila* orthologs (TERT and AR). This resulted in 16 candidate genes that could be targeted with drugs, most of which were FDA-approved.

**Inhibitors selectively affect NF1-deficient *Drosophila* and human cells**

Repurposing existing drugs represents the most efficient route to develop new therapeutics. Each of the 17 drugs that target the *NF1* synthetic lethal partner genes were first tested in WT and NF1-KO cells (with the exclusion of AZT and Enzalutamide due to DM cells lacking

targets) using CellTiter-Glo assays to measure the viability after 48 h of treatment (**Fig. S2)**. Of the 15 drugs tested in DM cells, we selected the two autophagy inhibitors (CQ and Bafilomycin A1) for further study in human *NF1* mutant cells, as both showed a significant and consistent effect on reducing NF1-KO viability.

***Autophagy inhibitors selectively affect NF1-deficient Drosophila and human cells***

One of the strongest hits from the screen was *Atg8b*, which encodes a key component of the autophagy pathway. Autophagy is commonly inhibited experimentally using CQ, which is clinically used as an anti-malarial and shows anti-viral properties, and Bafilomycin A1. CQ functions to inhibit autophagy by blocking the binding of autophagosomes to lysosomes by diffusing into the lysosomes and altering the acidic environment, thereby inhibiting autophagic lysosomal degradation (HOMEWOOD *et al.* 1972). On the other hand, Bafilomycin A1 disrupts autophagic flux by independently inhibiting V-ATPase-dependent acidification and Ca-P60A/SERCA-dependent autophagosome-lysosome fusion (MAUVEZIN AND NEUFELD 2015). We focused on CQ because it is generally well tolerated and can inhibit autophagy *in vivo* at clinically achievable concentrations (LEVY *et al.* 2017), and Bafilomycin A1 because it is a potent inhibitor of autophagy (KOCATURK *et al.* 2019).

We tested whether CQ and Bafilomycin A1 would phenocopy the selective effect observed using genetic inhibition of *Atg8b* in *Drosophila* cells. Both WT and NF1-KO cells were treated with varying doses of CQ or Bafilomycin A1 and cell viability was measured using CellTiter-Glo assays. A significantly greater effect on NF1-KO cell viability was observed at multiple concentrations of each drug in serum free media after 48 h of treatment, further validating the interaction between autophagy and NF1 (**Fig. 5A and 5F**). Similarly, propidium iodide (PI) staining was increased in NF1-KO cells compared to WT in the presence of CQ indicating increased cell death (**Fig. 5B**); however, we note that this was observed only at high CQ concentrations in both cases.

To determine whether the selective effect of CQ and Bafilomycin A1 was conserved in human cells, we tested the effects of drug treatment on a panel of human *NF1* mutant cell lines. These included CRISPR/Cas9-generated $NF1^{+/-}$ and $NF1^{-/-}$ immortalized Schwann cells [unpublished data] and two pairs of immortalized Schwann cells (pair 1: ipnNF95.11C ($NF1^{-/+}$) and ipNF95.11b "C" ($NF1^{-/-}$), pair 2: ipNF09.4 ($NF1^{-/+}$) and ipNF05.5 ($NF1^{-/-}$)) derived from plexiform neurofibromas (LI *et al.* 2016). Both CQ and Bafilomycin A1 resulted in a significantly greater reduction in the viability of homozygous $NF1^{-/-}$ mutant cells compared to heterozygous $NF1^{+/-}$ controls after 48 h of treatment under serum free media conditions ($P < 0.05$) (**Fig. 5C-E, 5G-I**).

Together, these results demonstrate that NF1-deficient cells have vulnerability to disruption of the autophagy pathway that is conserved and reproducible between *Drosophila* and human Schwann cells derived from NF1-associated tumours. Not only does autophagy represent a promising pathway for exploiting for the potential treatment of NF1-associated tumours, but we identified CQ and Bafilomycin A1 as candidate drugs for the treatment of NF1 tumours.

***hTERT inhibition selectively affects NF1-deficient human cells***

In addition to the two autophagy inhibitors identified to alter NF1-KO viability, we tested the two drugs targeting genes without *Drosophila* orthologs (AZT and Enzalutamide) in the panel of human *NF1* mutant cells lines, using CellTiter-Glo assays after 48 h treatment (**Fig. S2**). AZT is an antiretroviral medication used to prevent and treat HIV/AIDS by acting as an inhibitor of telomerase activity. hTERT was identified as a potential candidate gene in the GO and semantic similarity analysis of the genome-wide screen candidate genes. In each of the three human *NF1* mutant cell lines, AZT resulted in a significant reduction in $NF1^{-/-}$ cell viability relative to $NF1^{+/-}$ controls after 48 h treatment in serum free media ($P < 0.05$; **Fig. 6A-C**). This highlights the potential for telomerase inhibition as a promising therapeutic target for the potential treatment of NF1-associated tumours.

***AR inhibition selectively affects NF1-deficient human cells***

Enzalutamide is a non-steroidal androgen receptor (AR) inhibitor used in the treatment of prostate cancer (Bethesda 2012). AR was identified as a potential candidate gene in the KEGG pathway enrichment analysis (cancer pathway) as having an interaction with heat shock proteins identified in the genome-wide screen. In two human NF1 mutant cell lines, Enzalutamide resulted in a significant reduction in $NF1^{-/-}$ cell viability relative to $NF1^{+/-}$ controls after 48 h treatment in serum free media ($P < 0.05$; **Fig. 6D-F**). Therefore, AR inhibition is a further potential therapeutic target in the treatment of NF1-associated tumours.

**CQ affects survival in a *Drosophila in vivo NF1* mutant model**

As CQ is FDA-approved, well tolerated, and showed a significant effect on NF1-KO cell viability, we chose to take this drug forward to determine synthetic lethality *in vivo*. *Drosophila* mutant flies show defective Ras signalling, which results in a number of neurobehavioral phenotypes (GOUZI *et al.* 2011; WALKER *et al.* 2013; BAI *et al.* 2018; KING *et al.* 2020; MOSCATO *et al.* 2020). For this study, we generated novel *dNf1* null mutant flies using CRISPR gene editing: $dNf1^{C1}$ (*dNF1* delAT162-163) and $dNf1^{C2}$ (*dNF1* indel (3bp del/7bp insertion) (**Fig. 7A**). Western blots using lysates prepared from adult heads from CRISPR mutants showed no

expression of NF1 (**Fig. 7B**). In addition, ELISAs showed a 4-fold increase in pERK/ERK of dNf1 mutants compared to WT flies (**Fig. 7C**).

To determine whether CQ affects survival in *NF1*-mutant *Drosophila*, we took two approaches. Firstly, we tested flies with pan-neuronal RNAi knock down of dNf1 (using *nSyb-Gal4*) compared to landing site controls on food containing CQ (35 mM). Secondly, we compared the effect of CQ (35 mM) on $dNf1^{C1}/dNf1^{C2}$ null mutant flies, the WT parental line (control), and $dNf1^{C1}/dNf1^{C2}$ + *nSyb-Gal4>UAS-dNf1* (re-expression of dNf1 from a *UAS-dNF1* transgene driven with a pan-neuronal (*nSyb-Gal4*) driver). In flies with dNf1 RNAi knockdown, CQ significantly reduced the survival time compared to CQ-treated landing site control flies, and untreated flies (**Fig. 7D**). Similarly, CQ resulted in increased lethality of $dNf1^{C1}/dNf1^{C2}$ mutants compared to the WT parental line. Furthermore, we were able to rescue the CQ sensitivity of *dNf1* mutant flies by re-expression of dNf1 from a *UAS-dNF1* transgene (**Fig. 7E**). Together, these results demonstrate that *dNf1* mutant flies have vulnerability to disruption of the autophagy pathway, as shown to be conserved and reproducible in *Drosophila* NF1-KO cells and human Schwann cells derived from NF1-associated tumours. This further highlights the autophagy pathway as a target for the potential treatment of NF1-associated tumours, with CQ as a candidate drug.

**Selumetinib enhances to viability effect of CQ**

Selumetinib, a MEK1/2 inhibitor, is currently the only FDA-approved drug for the treatment of tumours associated with neurofibromatosis (MARKHAM AND KEAM 2020). We treated *Drosophila* S2R+ WT and NF1-KO cells with Selumetinib (10 μM) +/- CQ (1 mM) for 48 h in serum free media and performed CellTiter-Glo assays to measure cell viability (**Fig. 8A**). When treating cells with Selumetinib alone, a significant decrease in viability was observed in both WT and NF1-KO cells ($P < 0.05$), with no significant difference in viability observed between WT and NF1-KO. Similar to our earlier findings (**Fig. 5B**), treatment of cells with CQ alone resulted in a significant decrease in NF1-KO viability relative to WT cells ($P < 0.01$). When Selumetinib was combined with CQ, we see a further reduction in NF1-KO, but not WT, viability relative to the CQ only NF1-KO cells ($P < 0.05$), indicating that Selumetinib enhances the effects of CQ on *Drosophila* NF1-KO cell viability.

## DISCUSSION

Using *Drosophila* NF1 mutant cells as a model, we applied the method of synthetic lethal screening to identify candidate drug targets to treat NF1-deficient tumours. After statistical enrichment analysis of the 54 high confidence candidate genes, we further assessed a total of 72 candidate synthetic lethal partner genes to NF1 using VDA as an additional combinatorial screening method. This resulted in a list of 22 candidate genes that resulted in a >10% decrease in NF1-KO viability and were druggable targets. After further filtering of these targets to select those not previously identified as having a lethal interaction with NF1, we screened 15 existing drugs targeting the candidate genes in *Drosophila* NF1-KO and WT cells, noting that the autophagy inhibitors CQ and Bafilomycin A1 resulted in a significant reduction in NF1-KO cell viability. Notably, this effect was conserved in a panel of human NF1 mutant cell lines. The drugs AZT and Enzalutamide were also found to selectively reduce NF1 mutant cell viability in the human cell lines. Finally, we showed that the effect of CQ was conserved in a *Drosophila NF1*-mutant *in vivo* model. The results of this study highlight two key points: 1) the use of *Drosophila* cells as a model to screen for drugs specifically targeting *NF1* mutant cells was highly successful as the candidate interactions were conserved across a panel of human *NF1* mutant cells and an *in vivo* fly *NF1* mutant model, and 2) NF1-deficient cells have vulnerability to disruption of the autophagy pathway, telomerase activity, and AR activity. Not only do these pathways represent promising targets for exploiting for the potential treatment of NF1-associated tumours, but we identified CQ, Bafilomycin A1, AZT, and Enzalutamide as candidate drugs for the treatment of NF1 tumours.

We have previously reported the success of a synthetic screening method similar to the one used in this study, which combines CRISPR genome editing with RNAi (HOUSDEN *et al.* 2015; NICHOLSON *et al.* 2019). This approach has several advantages over the use of multiple RNAi reagents to perform combinatorial screens in *Drosophila* cells, including a reduction in the noise associated with dual RNAi screening, a homogenous population of null mutants, and in-depth characterisation of the mutant cell line prior to screening. Furthermore, previous screening methods have required a laborious secondary screen and further validation of candidate genes; however, using the CRISPR-RNAi combinatorial screening method in the present study, we could quickly identify the most robust candidates, which is reflected in the fact that we validated a high percentage of our candidate genes using VDA. In addition, we validated two of the most effective drugs (CQ and Bafilomycin A1) through to a panel of mammalian cell models of NF1. Therefore, screening in *Drosophila* cells as a model organism was rapidly translated to the identification of clinically relevant potential drug targets, as shown

previously (HOUSDEN *et al.* 2015). Finally, by performing the screen in *Drosophila* cells, this increases the likelihood of reproducible effects in mammalian models.

We identified *Atg8b* as a synthetic lethal partner to *NF1* in the genome-wide synthetic lethal screen, which was then validated in the VDA combinatorial screen. Atg8b (human ortholog: GABARAP) is an autophagy-related gene located in the autophagosome. Autophagy is the process where damaged organelles and unfolded proteins are sequestered into autophagosomes in the cytoplasm, which then undergo fusion with lysosomes (autolysosomes) resulting in degradation of the intracellular components (ZHANG *et al.* 2013). This is important in the regulation of cell growth, maturation, and death. In cancer, autophagy is reported to take on two roles: 1) degradation of damaged organelles and recycling of macromolecules to maintain a stable cellular environment, which prevents the formation of tumours (MIZUSHIMA *et al.* 2008); and 2) aiding in cancer cell survival in response to growth-limiting conditions, contributing to tumorigenesis (O'DONOVAN *et al.* 2011). Furthermore, autophagy has been widely reported to promote cancer cell survival through a drug resistance mechanism (O'DONOVAN *et al.* 2011; PENG *et al.* 2014). Therefore, targeting the autophagy pathway is a potential therapeutic option in the treatment of cancer.

As *Atg8b* was found to be a consistent and reproducible synthetic lethal partner gene to NF1, we hypothesized that inhibition of autophagy would have a similar lethal effect on NF1-deficient cell viability. The first inhibitor, CQ, is a widely used anti-malarial that functions to inhibit autophagy by blocking the binding of autophagosomes to lysosomes by diffusing into the lysosomes and altering the acidic environment, thereby inhibiting autophagic lysosomal degradation (HOMEWOOD *et al.* 1972). Previous studies have shown that CQ has anti-tumour properties in several types of cancer, including glioblastoma (GOLDEN *et al.* 2014; ZANOTTO-FILHO *et al.* 2015), hepatocellular carcinoma (MEI *et al.* 2015), prostate cancer (FARROW *et al.* 2014), breast cancer (LEFORT *et al.* 2014), and pancreatic cancer (YANG AND KIMMELMAN 2014). Similarly, we found that CQ significantly reduced NF1-KO cell viability relative to WT S2R+ cells across a range of concentrations under conditions where autophagy is induced (serum starvation of cells). This effect of CQ was conserved across a panel of three human NF1-deficient cell lines, two of which were derived from patient neurofibromas, as well as in an *in vivo* fly model of deficient NF1. Therefore, CQ shows great potential as an anti-tumour therapy in NF1-associated tumours. However, whilst there is a vast array of evidence for the efficacy and safety of CQ, the underlying mechanisms of the tumour suppressive actions of CQ remain to be determined. One potential mechanism is that under starvation conditions, such as those used in this study, a reduction in glucose transport results in a release of mTOR inhibition of the ULK1 complex, inducing vesicle nucleation and facilitating the process of

autophagy. Inhibition of the lysosome using CQ has been shown inhibit tumour growth and induce tumour cell death *in vitro* (ENG *et al.* 2016; JIA *et al.* 2017). However, why is it that NF1 mutant cells are more susceptible to autophagy inhibition with CQ? RAS has previously been shown to regulate autophagic flux (SCHMUKLER *et al.* 2014). In addition, cancers associated with RAS mutations have been reported to be dependent on autophagy, although this appears to be tumour cell line dependent (GUO *et al.* 2011; MORGAN *et al.* 2014). Therefore, cancers with aberrant RAS activity can be more susceptible to autophagy inhibition with CQ.

The second autophagy inhibitor that we screened was Bafilomycin A1, a macrolide antibiotic that disrupts autophagic flux by independently inhibiting V-ATPase-dependent acidification and Ca-P60A/SERCA-dependent autophagosome-lysosome fusion (MAUVEZIN AND NEUFELD 2015). Although some studies have shown Bafilomycin to promote cancer cell apoptosis, its toxicity potential has limited its medical applications (LEVY *et al.* 2017). We found that Bafilomycin A1 selectively reduced NF1-KO cell viability relative to WT controls at very low concentrations (0.1 fM – 3.2 fM), with little effect on WT cell viability. This effect was also conserved in the panel of three human NF1-defiicent cell lines at concentrations <10 nM. Similar results have been observed in paediatric B-cell lymphoblastic leukaemia cells (YUAN *et al.* 2015) and pancreatic cancer cells (OHTA *et al.* 1998). Regarding the mechanism of Bafilomycin A1, it has been reported to inhibit both late-stage autophagy and early-stage autophagy by activating mTOR and attenuating formation of the Beclin 1-Vps34 complex (YUAN *et al.* 2015). Interestingly, Atg6 (Beclin 1) was also identified as a synthetic lethal partner for NF1 in our screen.

Ras signalling is implicated in autophagy regulation. NF1 functions as a RasGAP (GTPase-activating protein), which facilitates Ras inactivation by enabling its GTPase activity (DOWNWARD 2003). In NF1-associated tumours, NF1 expression is downregulated, resulting in aberrant Ras activity and upregulation of the PI3K/Akt/mTOR1 pathway. Therefore, aberrant Ras activity is expected to negatively regulate autophagy; however, Ras is implicated in many signalling pathway and so it has a multifaceted role in autophagy regulation. For example, Ras also activates the Raf-1/MEK1/2/ERK and Rac1/MKK7/JNK signalling pathways, both of which are known to activate autophagy (SCHMUKLER *et al.* 2014). Therefore, we speculate that aberrant Ras activity in NF1-deficient cells results in the initiation of autophagy, and that inhibition of this pathway has anti-tumour effects. When combining our data on the effects of CQ and Bafilomycin A1, we provide strong evidence for inhibition of the autophagy pathway as a target in the treatment of NF1-associated tumours.

Furthermore, inhibition of autophagy with CQ increased the sensitivity of *Drosophila* NF1-KO cells to MEK1/2 inhibition with Selumetinib. Selumetinib is currently the only FDA-approved drug for the treatment of tumours associated with neurofibromatosis (MARKHAM AND KEAM 2020). The phase 2 trial (SPRINT) for the use of Selumetinib in plexiform neurofibromas reported clinically meaningful improvements in 71% of patients (GROSS *et al.* 2020), prompting its FDA approval for patients ages 2 to 18 years with neurofibromatosis type I who have symptomatic, inoperable plexiform neurofibromas. However, there are some toxicity effects related to long-term MEK inhibition (GROSS *et al.* 2020). Our data implies that autophagy inhibition via CQ could be an effective adjunctive therapy for NF1-associated tumours. This is in line with a previous study, which showed that combined inhibition of MEK1/2 plus autophagy had a synergistic anti-proliferative effect in pancreatic ductal adenocarcinoma cell lines, which display aberrant K-Ras activity, as well as patient-derived pancreatic ductal adenocarcinoma xenograft tumours in mice (KINSEY *et al.* 2019).

GO and KEGG pathway enrichment analysis of our list of genes identified as having a synthetic lethal interaction with NF1 identified two genes without fly orthologs, hTERT and AR. As both have been targeted in anti-cancer therapies, we decided to screen inhibitors of these two candidate genes in the panel of human NF1-deficient cell lines.

The GO term “telomerase holoenzyme complex assembly” (GO:1905323) was significantly enriched in the GO enrichment analysis of the candidate gene list from the screen (FDR adjusted P Value = 0.0059). AZT is an inhibitor of telomerase, which is a specialised reverse transcriptase (RT) that maintains telomeric length. hTERT encodes the functional catalytic component of the enzyme. The human holoenzyme telomerase is highly expressed in embryonic cells and is then repressed during adulthood; however, the enzyme is re-expressed in approximately 85% of solid tumours (GOMEZ *et al.* 2012), which has prompted studies to inhibit telomerase with the HIV RT AZT. AZT binds to telomeres, inhibits telomerase, and promotes tumour cell apoptosis (TEJERA *et al.* 2001; FALCHETTI *et al.* 2005; FANG AND BELAND 2009). We found that in all three human *NF1*$^{-/-}$ cell lines, AZT resulted in a significant reduction in cell viability across a range of concentrations, with little effect on *NF1*$^{+/-}$ cells at concentrations <500 µM. We hypothesize that the mechanism by which AZT selectively kills *NF1*$^{-/-}$ cells is due to the increased expression of the enzyme in *NF1*-deficient cells; however, further study is required to determine this.

KEGG pathway analysis of the candidate gene list from the screen identified AR to interact with several heat shock proteins from the screen in cancer signalling pathways. Furthermore, AR activation is downstream of the Ras-MEK-ERK1/2 pathway, with activation resulting in the

increased expression of several candidate genes that are synthetic lethal partners to NF1, namely, EGFR and hTERT. Therefore, AR inhibition was an attractive target in NF1-deficient cells. Enzalutamide is a second generation AR inhibitor used in the clinic to treat prostate cancer; it blocks several key steps in the AR signalling pathway including androgen binding to the AR, nuclear translocation of activated AR, and binding of activated AR to DNA (SCOTT 2018). We found that in two human *NF1*$^{-/-}$ cell lines, Enzalutamide resulted in a significant reduction in cell viability across a range of concentrations, with little effect on *NF1*$^{+/-}$ cells at concentrations <10 μM. Further study is required to elucidate the mechanism by which Enzalutamide selectively kills *NF1*$^{-/-}$ cells.

In conclusion, combinatorial screening in CRISPR-generated *Drosophila* NF1-KO cells with RNAi resulted in the identification of four potential candidate drugs for the treatment of NF1-associated tumours. The conservation of the synthetic lethal interactions between *Drosophila* and human NF1 mutant cells demonstrates the robustness of our combinatorial screening method. Finally, the use of a range of bioinformatic techniques allows identification of potential drug targets that are not conserved in *Drosophila*, further increasing the utility of the approach.

## METHODS

### Cell culture

*Drosophila* Schneider (S2R+) cells, both WT and NF1-KO, were cultured at 25°C in Schneider's media (Gibco) containing 1% antibiotic (Gibco) and 10% fetal bovine serum (Gibco). Human cell lines included *NF1*$^{-/+}$ and *NF1*$^{-/-}$ immortalised human Schwann cell (SC) lines, derived from the 02.3λ cell line from a healthy individual (FISHBEIN *et al.* 2007) using CRISPR/Cas9 gene editing to introduce *NF1* indels; *NF1*$^{-/-}$ CRISPR SCs have been shown to have *in vivo* tumourigenic potential in mice (unpublished data). In addition, we used two immortalised human SCs derived from plexiform neurofibromas from NF1 patients {Li, 2016 #45}, which included ipnNF95.11C (*NF1*$^{-/+}$) and ipNF95.11b'C' (*NF1*$^{-/-}$) cells (germline *NF1* mutation: c.1756delACTA), and ipNF09.4 (*NF1*$^{-/+}$) and ipNF05.5 (*NF1*$^{-/-}$) cells (germline *NF1* mutation: c.3456_3457insA). All human cell lines were cultured at 37℃ in 5% $CO_2$ in DMEM media (Merck) containing 1% antibiotic (Gibco) and 10% fetal bovine serum (Gibco). For ipnNF09.4 and ipNF05.5 cells, the media was also supplemented with 50 ng/ml neuregulin-1 (NRG-1) (Sigma).

### Generation of NF1-KO *Drosophila* cells

The NF1-KO cell line was generated as described previously (HOUSDEN *et al.* 2015; HOUSDEN *et al.* 2017c). Wild-type S2R+ cells were co-transfected with the pl018 plasmid to express Cas9 and the sgRNA (CGCTTCTCCCTTGTCATATC) and pAct-GFP plasmid to mark transfected cells. 5 days after transfection, individual cells with the highest 15% GFP signal were isolated and seeded into wells of 96-well plates using FACS. Single cells were cultured using conditioned media for approximately 3 weeks. DNA was then extracted from each candidate cell population and assessed using HRMA to identify those carrying mutations at the sgRNA target site. Positive candidates were then sequenced to confirm homozygous frame-shift mutations were present (**Fig. 1A**).

### Synthetic lethal screen

Screens were performed using WT S2R+ or NF1-KO cells as described previously using the genome-wide RNAi library from the Sheffield RNAi Screening Facility (SRSF). 10,000 cells were seeded into each library well in 10 µl serum free Schneider's *Drosophila* media. Plates were then incubated at room temperature for 45 minutes before addition of 35 µl media with

10% FBS. Libraries were incubated at 25°C for 5 days before CellTiter-Glo® assays were performed. Screens were performed in triplicate in each cell line.

Data were analysed by first normalising all values to the median of each row and column of the library plate to allow direct comparison between plates. Z-scores were then calculated for each RNAi reagent using the average and standard deviation of each replicate screen. Reagents were considered hits if the Z-score in at least 2/3 of replicates was below -1.5 in NF1-KO cells and above -1.5 in S2R+ cells.

**Statistical enrichment analysis**

Statistical enrichment analysis was used to identify additional candidates to those identified in the screen. Gene ontology (GO) and semantic similarity analysis was performed using the GOSemSim package in R (YU 2020). KEGG pathway analysis was performed using the KEGG Pathway Database (https://www.genome.jp/kegg/pathway.html). In addition, STRING was used to perform protein-protein interaction functional enrichment analysis (https://string-db.org/).

**Variable dose analysis (VDA)**

VDA is an RNAi-based method in which each cell within a population receives a different dose of shRNA. The relative knockdown efficiency of each cell is then measured with a fluorescent reporter. On the day of transfection S2R+ (WT) and NF1-KO cells were plated at 1 x $10^4$ cell/100 µl culture media, per well of a 96-well plate. Cells were incubated at 25℃ for 40 minutes to allow adhesion. Cells were then transfected with 40 ng actin-GFP and 160 ng shRNA expression plasmid using 0.6 µl FuGENE® HD transfection reagent in a total volume of 10ul. We used a positive (*thread*, an apoptosis inhibitor that induces cell death when inhibited) and negative (*white*, known to have no viability effect in these cells) shRNA on each plate for normalisation of data. Plates were then sealed and incubated for 4 days at 25℃ in a humidifying chamber.

Flow cytometry was used to identify GFP-positive cells (transfection efficiency). A Matlab script was used to determine the area under the curve (AUC), normalised to the positive and negative control, as a measure of transfected cell viability. More detailed protocol and data analysis information can be found in Sierzputowska et al. (SIERZPUTOWSKA *et al.* 2018).

**CellTiter-Glo® assays**

The CellTiter-Glo® assay (Promega; G7570) is a luminescent viability assay based on the quantification of ATP, which is an indicator of metabolically active cells. All cells were plated

in white 384-well plates at a seeding density of 5 x $10^3$ cells/25 µl culture media in either complete or serum free (SF) media. S2R+ cells were left to adhere for 40 mins at 25℃ and human cells were left to adhere for 4 h at 37℃ in 5% $CO_2$ before treatment. Cells were treated with 250 nl per well of each drug (CQ, Bafilomycin A1, AZT, Enzalutamide, and Selumetinib) in PBS at varying concentrations in replicates of 5-8 using the Mosquito LV Genomics (SPT Labtech) and incubated for 48 h. The CellTiter-Glo® assay was then performed according to the manufacturer's instructions, and luminescence was measured using a plate reader (TECAN Infinite M200 Pro).

### *Drosophila* Husbandry and Stocks

Flies were cultured on cornmeal/agar food medium according to standard protocol and housed at 25°C.

The *Nf1*$^{C1}$ and *Nf1*$^{C2}$ mutant fly lines were generated by CRISPR/Cas9 (REN *et al.* 2013). using the sgRNA line: *y[1] sc[*] v[1] sev[21]; P{y[+t7.7] v[+t1.8]=TKO.GS01796}attP40* (GS01796 sgRNA sequence: CGCTTCTCCCTTGTCATATC) and a germline source of Cas9: *y[1] M{w[+mC]=nos-Cas9.P}ZH-2A w[*]* (Bloomington Stock #54591). The *UAS-dNf1* transgene encodes full-length *dNf1* cDNA corresponding to the RF isoform with addition of introns 9 and 10 and was previously published (WALKER *et al.* 2006). RNAi and landing site control lines were obtained from the Transgenic RNAi Project (TRiP) and Vienna *Drosophila* RNAi Center: *dNf1 RNAi* lines: P{TRiP.JF01866}attP2 JF01866 (Bloomington Stock: 25845), P{KK101909}VIE-260B (VDRC #109637); control crosses consisted of empty attP landing site lines: P{y[+t7.7]=CaryP}attP2 (Bloomington Stock: 36303) and VIE-260B (VDRC #60100). *UAS-dicer2* was included to potentiate the RNAi effect (DIETZL *et al.* 2007): *P{w[+mC]=UAS-Dcr-2.D}2* and *P{w[+mC]=UAS-Dcr-2.D}10* (Bloomington: 24650 and 24651). Male flies were used for all experiments.

### Assessing drug sensitivity in flies

Flies were raised on standard fly food and kept at 25°C. For testing drugs, adult flies were transferred to Formula 4-24 Instant *Drosophila* Medium (Carolina Biological) prepared using water (control) or 35 µM chloroquine (chloroquine diphosphate; Sigma C6628) in water. For each genotype, three replicates of 20 flies were added to each condition and kept at 25°C. Flies were monitored periodically to assess lethality. Survival was reported as the percent of flies still alive at each time point.

## Western Blotting

Expression of Nf1 in S2R+ cells was assessed using Western blotting. Lysates were prepared in RIPA buffer and analysed as detailed below. Expression of Nf1 in adult flies was assessed using immunoprecipitation (IP) followed by western blotting. Lysates of heads from 2 to 3-day old adult flies were prepared using IP buffer (50 mM Tris-HCl pH 7.5, 125 mM NaCl, 1.5 mM MgCl2, 0.2% NP-40, 5% glycerol) supplemented with protease inhibitors (Complete Protease Inhibitor Cocktail, Sigma) and phosphatase inhibitors (NaF/Na3VO4/β-glycerophosphate). Immunoprecipitations were performed using 400 µg of total protein in 1 ml IP buffer incubated with 200 µl of mAb21 anti-Nf1 monoclonal antibody supernatant (THE *et al.* 1997) for 1 h at 4°C. Immunocomplexes were precipitated with a mix of Protein A- and Protein G-Sepharose beads (1:1, Sigma) for 1 h at 4°C before washing three times with IP buffer and denaturing with 2× SDS sample buffer. Lysates and immunoprecipitates were resolved on NuPAGE 3–8% Tris-Acetate (for Nf1) or NuPAGE 4–12% Bis-Tris gels (pERK/ERK/β-tubulin). After transfer to nitrocellulose membranes, blots were processed according to the Odyssey CLx protocol (LI-COR). Antibodies used for immunoblotting: anti-Nf1 (mouse, mAb21, 1:10), anti-β-tubulin (mouse, Developmental Studies Hybridoma Bank E7, 1:10,000), anti-mouse IRDye secondary antibody (goat, Invitrogen, A32730, 1:10,000), and anti-rabbit IRDye (donkey, Invitrogen, A10043, 1:10,000) secondary antibody.

## ELISA

pERK/ERK levels were assessed using the ERK1/2 (pT202/Y204) + ERK1/2 Total SimpleStep ELISA Kit from Abcam (ab176660). Briefly, 20 *Drosophila* heads were lysed in 60 µL of Cell Extraction Buffer with Enhancer in 1.5 mL Eppendorf tubes with a pestle to yield a protein concentration of 10 µg/µL. Lysates were spun for 5 minutes at 13k rpm at 4°C and transferred to new tubes and diluted to 0.5 µg/µL (12.5 µL of lysate plus 237.5 µL of buffer). Each sample was run in duplicate using 50 µL of diluted protein for a total of 25 µg per sample. Samples were incubated with either p-ERK1/2 or total ERK1/2 antibody cocktail for 1 hour at room temperature with agitation prior to colour development driven by the addition of TMB substrate. After adding the stop solution, the OD was read at 450 nm using a SpectraMax Plus microplate reader. pERK/total ERK ratio was determined by dividing the pERK reading by the total ERK reading. Error bars represent the standard deviation. A paired, two-tailed t-test was performed to determine significance; *P < 0.05.

## COMPETING INTERESTS

The authors declare no competing interests.

## ACKNOWLEDGEMENTS

Research support was provided by the Medical Research Council (MR/V009583/1) and the University of Exeter (B.E.H), and NIH R21 NS096402 and DOD-NFRP W81XWH-16-1-0220 (J.A.W.). NP is an investigator of HHMI. We thank the Sheffield RNAi Screening Facility, Biomedical Sciences, University of Sheffield, supported by the Wellcome Trust (grant reference number 084757) for providing RNAi libraries.

## REFERENCES

Bethesda, 2012 Enzalutamide in *Bethesda (MD). National Institute of Diabetes and Digestive and Kidney Diseases. LiverTox: Clinical and Research Information on Drug-Induced Liver Injury.* https://www.ncbi.nlm.nih.gov/books/NBK548070/.

Bai, L., Y. Lee, C. T. Hsu, J. A. Williams, D. Cavanaugh *et al.*, 2018 A Conserved Circadian Function for the Neurofibromatosis 1 Gene. Cell Rep 22: 3416-3426.

Baldo, F., A. Magnolato, E. Barbi and I. Bruno, 2021 Selumetinib side effects in children treated for plexiform neurofibromas: first case reports of peripheral edema and hair color change. BMC Pediatr 21: 67.

Dietzl, G., D. Chen, F. Schnorrer, K. C. Su, Y. Barinova *et al.*, 2007 A genome-wide transgenic RNAi library for conditional gene inactivation in Drosophila. Nature 448: 151-156.

Downward, J., 2003 Targeting RAS signalling pathways in cancer therapy. Nat Rev Cancer 3: 11-22.

Eng, C. H., Z. Wang, D. Tkach, L. Toral-Barza, S. Ugwonali *et al.*, 2016 Macroautophagy is dispensable for growth of KRAS mutant tumors and chloroquine efficacy. Proc Natl Acad Sci U S A 113: 182-187.

Evans, D. G., E. Howard, C. Giblin, T. Clancy, H. Spencer *et al.*, 2010 Birth incidence and prevalence of tumor-prone syndromes: estimates from a UK family genetic register service. Am J Med Genet A 152A: 327-332.

Falchetti, A., A. Franchi, C. Bordi, C. Mavilia, L. Masi *et al.*, 2005 Azidothymidine induces apoptosis and inhibits cell growth and telomerase activity of human parathyroid cancer cells in culture. J Bone Miner Res 20: 410-418.

Fang, J. L., and F. A. Beland, 2009 Long-term exposure to zidovudine delays cell cycle progression, induces apoptosis, and decreases telomerase activity in human hepatocytes. Toxicol Sci 111**:** 120-130.

Farrow, J. M., J. C. Yang and C. P. Evans, 2014 Autophagy as a modulator and target in prostate cancer. Nat Rev Urol 11**:** 508-516.

Fishbein, L., X. Zhang, L. B. Fisher, H. Li, M. Campbell-Thompson *et al.*, 2007 In vitro studies of steroid hormones in neurofibromatosis 1 tumors and Schwann cells. Mol Carcinog 46**:** 512-523.

Golden, E. B., H. Y. Cho, A. Jahanian, F. M. Hofman, S. G. Louie *et al.*, 2014 Chloroquine enhances temozolomide cytotoxicity in malignant gliomas by blocking autophagy. Neurosurg Focus 37**:** E12.

Gomez, D. E., R. G. Armando and D. F. Alonso, 2012 AZT as a telomerase inhibitor. Front Oncol 2**:** 113.

Gouzi, J. Y., A. Moressis, J. A. Walker, A. A. Apostolopoulou, R. H. Palmer *et al.*, 2011 The receptor tyrosine kinase Alk controls neurofibromin functions in Drosophila growth and learning. PLoS Genet 7**:** e1002281.

Gross, A. M., P. L. Wolters, E. Dombi, A. Baldwin, P. Whitcomb *et al.*, 2020 Selumetinib in Children with Inoperable Plexiform Neurofibromas. N Engl J Med 382**:** 1430-1442.

Guo, J. Y., H. Y. Chen, R. Mathew, J. Fan, A. M. Strohecker *et al.*, 2011 Activated Ras requires autophagy to maintain oxidative metabolism and tumorigenesis. Genes Dev 25**:** 460-470.

Gutmann, D. H., R. E. Ferner, R. H. Listernick, B. R. Korf, P. L. Wolters *et al.*, 2017 Neurofibromatosis type 1. Nat Rev Dis Primers 3**:** 17004.

Homewood, C. A., D. C. Warhurst, W. Peters and V. C. Baggaley, 1972 Lysosomes, pH and the anti-malarial action of chloroquine. Nature 235**:** 50-52.

Housden, B. E., Z. Li, C. Kelley, Y. Wang, Y. Hu *et al.*, 2017a Improved detection of synthetic lethal interactions in Drosophila cells using variable dose analysis (VDA). Proc Natl Acad Sci U S A 114**:** E10755-E10762.

Housden, B. E., M. Muhar, M. Gemberling, C. A. Gersbach, D. Y. Stainier *et al.*, 2017b Loss-of-function genetic tools for animal models: cross-species and cross-platform differences. Nat Rev Genet 18**:** 24-40.

Housden, B. E., H. E. Nicholson and N. Perrimon, 2017c Synthetic Lethality Screens Using RNAi in Combination with CRISPR-based Knockout in Drosophila Cells. Bio Protoc 7.

Housden, B. E., A. J. Valvezan, C. Kelley, R. Sopko, Y. Hu *et al.*, 2015 Identification of potential drug targets for tuberous sclerosis complex by synthetic screens combining CRISPR-based knockouts with RNAi. Sci Signal 8**:** rs9.

Jia, L., J. Wang, T. Wu, J. Wu, J. Ling *et al.*, 2017 In vitro and in vivo antitumor effects of chloroquine on oral squamous cell carcinoma. Mol Med Rep 16**:** 5779-5786.

Kaelin, W. G., Jr., 2005 The concept of synthetic lethality in the context of anticancer therapy. Nat Rev Cancer 5**:** 689-698.

King, L. B., T. Boto, V. Botero, A. M. Aviles, B. M. Jomsky *et al.*, 2020 Developmental loss of neurofibromin across distributed neuronal circuits drives excessive grooming in Drosophila. PLoS Genet 16**:** e1008920.

Kinsey, C. G., S. A. Camolotto, A. M. Boespflug, K. P. Guillen, M. Foth *et al.*, 2019 Protective autophagy elicited by RAF-->MEK-->ERK inhibition suggests a treatment strategy for RAS-driven cancers. Nat Med 25**:** 620-627.

Kocaturk, N. M., Y. Akkoc, C. Kig, O. Bayraktar, D. Gozuacik *et al.*, 2019 Autophagy as a molecular target for cancer treatment. Eur J Pharm Sci 134**:** 116-137.

Lawrence, M. S., P. Stojanov, C. H. Mermel, J. T. Robinson, L. A. Garraway *et al.*, 2014 Discovery and saturation analysis of cancer genes across 21 tumour types. Nature 505**:** 495-501.

Lee, H., C. J. McManus, D. Y. Cho, M. Eaton, F. Renda *et al.*, 2014 DNA copy number evolution in Drosophila cell lines. Genome Biol 15**:** R70.

Lefort, S., C. Joffre, Y. Kieffer, A. M. Givel, B. Bourachot *et al.*, 2014 Inhibition of autophagy as a new means of improving chemotherapy efficiency in high-LC3B triple-negative breast cancers. Autophagy 10**:** 2122-2142.

Levy, J. M. M., C. G. Towers and A. Thorburn, 2017 Targeting autophagy in cancer. Nat Rev Cancer 17**:** 528-542.

Li, H., L. J. Chang, D. R. Neubauer, D. F. Muir and M. R. Wallace, 2016 Immortalization of human normal and NF1 neurofibroma Schwann cells. Lab Invest 96**:** 1105-1115.

Lord, C. J., and A. Ashworth, 2017 PARP inhibitors: Synthetic lethality in the clinic. Science 355**:** 1152-1158.

Markham, A., and S. J. Keam, 2020 Selumetinib: First Approval. Drugs 80**:** 931-937.

Martin, G. A., D. Viskochil, G. Bollag, P. C. McCabe, W. J. Crosier *et al.*, 1990 The GAP-related domain of the neurofibromatosis type 1 gene product interacts with ras p21. Cell 63**:** 843-849.

Mauvezin, C., and T. P. Neufeld, 2015 Bafilomycin A1 disrupts autophagic flux by inhibiting both V-ATPase-dependent acidification and Ca-P60A/SERCA-dependent autophagosome-lysosome fusion. Autophagy 11**:** 1437-1438.

Mei, L., Y. Chen, Z. Wang, J. Wang, J. Wan *et al.*, 2015 Synergistic anti-tumour effects of tetrandrine and chloroquine combination therapy in human cancer: a potential antagonistic role for p21. Br J Pharmacol 172**:** 2232-2245.

Mizushima, N., B. Levine, A. M. Cuervo and D. J. Klionsky, 2008 Autophagy fights disease through cellular self-digestion. Nature 451**:** 1069-1075.

Morgan, M. J., G. Gamez, C. Menke, A. Hernandez, J. Thorburn *et al.*, 2014 Regulation of autophagy and chloroquine sensitivity by oncogenic RAS in vitro is context-dependent. Autophagy 10**:** 1814-1826.

Moscato, E. H., C. Dubowy, J. A. Walker and M. S. Kayser, 2020 Social Behavioral Deficits with Loss of Neurofibromin Emerge from Peripheral Chemosensory Neuron Dysfunction. Cell Rep 32**:** 107856.

Nicholson, H. E., Z. Tariq, B. E. Housden, R. B. Jennings, L. A. Stransky *et al.*, 2019 HIF-independent synthetic lethality between CDK4/6 inhibition and VHL loss across species. Sci Signal 12.

O'Donovan, T. R., G. C. O'Sullivan and S. L. McKenna, 2011 Induction of autophagy by drug-resistant esophageal cancer cells promotes their survival and recovery following treatment with chemotherapeutics. Autophagy 7**:** 509-524.

Ohta, T., H. Arakawa, F. Futagami, S. Fushida, H. Kitagawa *et al.*, 1998 Bafilomycin A1 induces apoptosis in the human pancreatic cancer cell line Capan-1. J Pathol 185**:** 324-330.

Peng, X., F. Gong, Y. Chen, Y. Jiang, J. Liu *et al.*, 2014 Autophagy promotes paclitaxel resistance of cervical cancer cells: involvement of Warburg effect activated hypoxia-induced factor 1-alpha-mediated signaling. Cell Death Dis 5**:** e1367.

Rasmussen, S. A., Q. Yang and J. M. Friedman, 2001 Mortality in neurofibromatosis 1: an analysis using U.S. death certificates. Am J Hum Genet 68**:** 1110-1118.

Ren, X., J. Sun, B. E. Housden, Y. Hu, C. Roesel *et al.*, 2013 Optimized gene editing technology for Drosophila melanogaster using germ line-specific Cas9. Proc Natl Acad Sci U S A 110**:** 19012-19017.

Ryan, C. J., I. Bajrami and C. J. Lord, 2018 Synthetic Lethality and Cancer - Penetrance as the Major Barrier. Trends Cancer 4**:** 671-683.

Schmukler, E., Y. Kloog and R. Pinkas-Kramarski, 2014 Ras and autophagy in cancer development and therapy. Oncotarget 5**:** 577-586.

Scott, L. J., 2018 Enzalutamide: A Review in Castration-Resistant Prostate Cancer. Drugs 78**:** 1913-1924.

Sierzputowska, K., C. R. Baxter and B. E. Housden, 2018 Variable Dose Analysis: A Novel High-throughput RNAi Screening Method for Drosophila Cells. Bio Protoc 8**:** e3112.

Simanshu, D. K., D. V. Nissley and F. McCormick, 2017 RAS Proteins and Their Regulators in Human Disease. Cell 170**:** 17-33.

Szklarczyk, D., A. L. Gable, D. Lyon, A. Junge, S. Wyder *et al.*, 2019 STRING v11: protein-protein association networks with increased coverage, supporting functional discovery in genome-wide experimental datasets. Nucleic Acids Res 47**:** D607-D613.

Tejera, A. M., D. F. Alonso, D. E. Gomez and O. A. Olivero, 2001 Chronic in vitro exposure to 3'-azido-2', 3'-dideoxythymidine induces senescence and apoptosis and reduces tumorigenicity of metastatic mouse mammary tumor cells. Breast Cancer Res Treat 65**:** 93-99.

The, I., G. E. Hannigan, G. S. Cowley, S. Reginald, Y. Zhong *et al.*, 1997 Rescue of a Drosophila NF1 mutant phenotype by protein kinase A. Science 276**:** 791-794.

Valvezan, A. J., M. Turner, A. Belaid, H. C. Lam, S. K. Miller *et al.*, 2017 mTORC1 Couples Nucleotide Synthesis to Nucleotide Demand Resulting in a Targetable Metabolic Vulnerability. Cancer Cell 32**:** 624-638 e625.

Walker, J. A., J. Y. Gouzi, J. B. Long, S. Huang, R. C. Maher *et al.*, 2013 Genetic and functional studies implicate synaptic overgrowth and ring gland cAMP/PKA signaling defects in the Drosophila melanogaster neurofibromatosis-1 growth deficiency. PLoS Genet 9**:** e1003958.

Walker, J. A., A. V. Tchoudakova, P. T. McKenney, S. Brill, D. Wu *et al.*, 2006 Reduced growth of Drosophila neurofibromatosis 1 mutants reflects a non-cell-autonomous requirement for GTPase-Activating Protein activity in larval neurons. Genes Dev 20**:** 3311-3323.

Yang, A., and A. C. Kimmelman, 2014 Inhibition of autophagy attenuates pancreatic cancer growth independent of TP53/TRP53 status. Autophagy 10**:** 1683-1684.

Yu, G., 2020 Gene Ontology Semantic Similarity Analysis Using GOSemSim. Methods Mol Biol 2117**:** 207-215.

Yuan, N., L. Song, S. Zhang, W. Lin, Y. Cao *et al.*, 2015 Bafilomycin A1 targets both autophagy and apoptosis pathways in pediatric B-cell acute lymphoblastic leukemia. Haematologica 100**:** 345-356.

Zanotto-Filho, A., E. Braganhol, K. Klafke, F. Figueiro, S. R. Terra *et al.*, 2015 Autophagy inhibition improves the efficacy of curcumin/temozolomide combination therapy in glioblastomas. Cancer Lett 358**:** 220-231.

Zhang, X. J., S. Chen, K. X. Huang and W. D. Le, 2013 Why should autophagic flux be assessed? Acta Pharmacol Sin 34**:** 595-599.

## TABLES

**Table 1. Selected top ranked hits from screens for NF1 synthetic lethal interactors**

| Gene Symbol | FBgn ID | Human ortholog | Delta-Z | Function |
|---|---|---|---|---|
| CG10516 | FBgn0036549 | SPSB3 | 3.74 | Protein degradation (inferred) |
| RpL13A | FBgn0037351 | RPL13A | 3.3 | Protein translation |
| Atg8b | FBgn0038539 | GABARAP | 2.6 | Autophagy |
| eIF3i | FBgn0015834 | EIF3I | 2.04 | Protein translation |
| Rpt3R | FBgn0037742 | PSMC4 | 1.87 | Proteosome regulation |
| Rbbp5 | FBgn0036973 | RBBP5 | 1.85 | Histone methylation |
| RpS6 | FBgn0261592 | RPS6 | 1.79 | Protein translation |
| Uba1 | FBgn0023143 | UBA1 | 1.76 | Ubiquitination |
| RpL34a | FBgn0039406 | RPL34 | 1.69 | Protein translation |
| geminin | FBgn0033081 | GMNN | 1.55 | DNA replication |

**Table 2. Candidate genes that decreased NF1-KO viability and were druggable targets without previous evidence of an interaction with NF1**

| Drug | Target: DM (Human) |
|---|---|
| Chloroquine* | Atg8b (GABARAP), RpS6 (RPS6) |
| EAD1 | Atg8b (GABARAP), RpS6 (RPS6) |
| Avapritinib* | Pvr (VEGFR and PDGFR) |
| Selumetinib* | Dsor1 (MEK, MAPKK) |
| Tazemetostat* | E(z) (EZH2) |
| Suramin* | Cul-1 (CUL1) |
| Metformin* | ND-MNLL (NDUFB1) |
| PYR41 | Uba1 (UBA1) |
| LB100 | Pp2A-29B (PPP2R1A and PPP2R1B) |
| Mitoxantrone* | Rac1 (RAC1) |
| Erdafitinib* | Bnl (FGFR2) |
| VLX1570 | Usp14 (USP14) |
| L-Thyroxine* | Fal (SAMHD1) |
| Atovaquone* | Mt:Cyt-B (MT:CYB) |
| Azidothymidine* | hTERT (no DM ortholog) |
| Enzalutamide* | AR (no DM ortholog) |
| Bafilomycin A1 | Atg8b (GABARAP), RpS6 (RPS6) |

*FDA-approved

## FIGURE LEGENDS

### Figure 1. Characterisation of NF1-deficient *Drosophila* cells.

**(A)** S2R+ cells were transfected with Cas9 and sgRNA designed to target a double-strand break to a region close to the 5' end of the *NF1* coding sequence. **(B)** Representative image of Western blot showing loss of neurofibromin in NF1-KO cells compared to WT S2R+ cells (two replicates performed). **(C)** Characterisation of *NF1* mutant cell size and proliferation rate. Bars indicate the average of at least eight biological replicates and error bars indicate SEM. (**P < 0.01 and *P < 0.05 as determined using paired, two-tailed t-tests. Baseline: n=60, Serum-free: n=50, Full-serum: n=42, Cell Counts: n=8).

### Figure 2. A network of synthetic lethal interaction for *Drosophila* NF1.

**(A)** Using the NF1-KO cells, we used a genome-wide dsRNA library to screen approximately 10000 genes, resulting in 134 genes identified as having a synthetic lethal interaction with *NF1*. **(B)** Summary of results from the synthetic lethal screen. Z-scores are plotted for NF1-KO cells on the vertical axis and WT S2R+ cells on the horizontal axis. The red box indicates the position of reagents selected as hits. **(C)** Correlation analysis of screen replicates indicating high data quality. Each bar represents the correlation coefficient from comparison between two screen replicates in WT or NF1-KO cells as indicated or between the median Z-scores for each cell line. **(D)** A synthetic lethal interaction network for *NF1*. Colours indicate approximate clustering into functional groups. Solid lines represent physical interactions within functional groups and dashed lines represent physical interactions between functional groups. (?) indicates relatively weak or inconsistent evidence for cluster functions.

### Figure 3. Statistical enrichment analysis of synthetic lethal screen candidate genes.

**(A)** Flow diagram to show the process of enrichment analysis. During the first stage, we identified GO terms that were significantly represented by the 54 candidate gene terms (FDR < 0.05). This resulted in 215 enriched terms in biological processes (BP), 43 enriched terms in molecular function (MF), and 79 enriched terms in cellular component (CC) subcategories. Semantic similarity between terms was visualised using the Revigo tool (http://revigo.irb.hr/), with an example shown in **(B)** for MF; semantic similarity was observed between "*histone methyltransferase activity (H3-K4 specific)"* and *"N-methyltransferase activity"*. Semantic similarity analysis of candidate gene GO terms with NF1 GO enriched terms is shown in Table S3b. Genes included in terms identified to have semantic similarity were screened for those that could be targeted by FDA-approved drugs, resulting in the addition of RAC1, EGFR, FGFR, EZH2, and hTERT. KEGG pathway enrichment analysis identified 15 pathways associated with the candidate gene list (three examples shown in **(C)**), which were used to

screen for additional genes located upstream/downstream of the candidate gene signalling pathways that could be targeted with FDA-approved drugs. This resulted in the identification of MYC, AR, CUL1, and mTOR (in addition to EGFR, which was identified in the GO analysis). Finally, we assessed protein-protein interactions of the individual genes in the screen using the String database (https://string-db.org/) to identify interactions with additional genes that could be targeted with FDA-approved drugs. This resulted in the identification of PDGFRA, RAF1, MEK, KRAS, MT-CYB, BECN1, RP, GFAP, SKP1, USP14, SAMHD1, and CDC37.

**Figure 4. Additional screening of candidate drug targets using VDA analysis.**

**(A)** Validation of the interactions between the indicated genes and NF1 using VDA assays. Bars indicate the average of at least 17 replicates (RpL13A: Obs n=24; Exp n=24, Atg8b: Obs n=22; Exp n=17, Rpt3R: Obs n=18; Exp n=18, Rbbp5: Obs n=24; Exp n=24, Uba1: Obs n=24; Exp n=24, CG17917: Obs n=24; Exp n=24, Hsp83: Obs n=24; Exp n=24; error bars indicate SEM. **(B)** VDA assays performed for all 72 candidate genes, with two shRNAs per gene, in WT S2R+ (black) and NF1-KO (white) cells. Shown is the best shRNA from the 59 genes that reduced NF1-KO viability by >10% relative to WT controls ranked in order of effect. **(C)** shRNA gene knockdowns that resulted in a >10% reduction in NF1-KO viability compared to WT controls and were druggable targets. Bars indicate the average of nine biological replicates and error bars indicate SEM. All 22 showed a significant reduction in NF1-KO viability relative to WT controls assessed using the Student's t-test (**P < 0.01).

**Figure 5. CQ and Bafilomycin A1 selectively affect NF1-deficient *Drosophila* and human cells.**

**(A)** Effect of CQ on viability of WT and NF1-KO *Drosophila* (DM) S2R+ cells after 48 h in serum free media (n=16). **(B)** Analysis of cell death using PI staining with CQ in WT and NF1-KO DM cells (n=4). **(C-E)** CQ significantly reduced $NF1^{-/-}$ cell viability (red line) relative to $NF1^{+/-}$ controls (black line) at varying doses in CRISPR/Cas9 SCs **(C)**, ipNF95.11b/ipNF95.11b cells **(D)**, and iPNF09.4/ipNF05.5 cells **(E)** after 48 h in serum free media (n=10-16). **(F)** Effect of Bafilomycin A1 on viability of WT and NF1-KO *Drosophila* (DM) S2R+ cells after 48 h in serum free media (n=16). **(G-I)** Bafilomycin A1 significantly reduced $NF1^{-/-}$ cell viability (red line) relative to $NF1^{+/-}$ controls (black line) at varying doses in CRISPR/Cas9 SCs **(G)**, ipNF95.11b/ipNF95.11b cells **(H)**, and iPNF09.4/ipNF05.5 cells **(I)** after 48 h in serum free media (n=10-16). In all cases, data represent the mean and error bars indicate SEM (**P < 0.01 and *P < 0.05 vs control; Student's t-test).

**Figure 6. AZT and Enzalutamide selectively affect NF1-deficient human cells.**

AZT significantly reduced *NF1*$^{-/-}$ cell viability (red line) relative to *NF1*$^{+/-}$ controls (black line) at varying doses in CRISPR/Cas9 SCs **(A)**, ipNF95.11b/ipNF95.11b cells **(B)**, and iPNF09.4/ipNF05.5 cells **(C)** after 48 h in serum free media (n=10-16). Enzalutamide significantly reduced *NF1*$^{-/-}$ cell viability (red line) relative to *NF1*$^{+/-}$ controls (black line) at varying doses in CRISPR/Cas9 SCs **(D)**, and ipNF95.11b/ipNF95.11b cells **(E)** after 48 h in complete media (n=10). In all cases, data represent the mean and error bars indicate SEM (**P < 0.01 and *P < 0.05 vs control; Student's t-test).

**Figure 7. CQ affects lethality in NF1-mutant *Drosophila in vivo.***

**(A)** We generated novel *dNf1* null mutants using CRISPR gene editing: *dNf1*$^{C1}$ (*dNF1* delAT162-163) and *dNf1*$^{C2}$ (*dNF1* indel (3bp del/7bp insertion). **(B)** Western blots of anti-dNf1 immunoprecipitates from lysates prepared from adult heads from CRISPR mutants showed no expression of Nf1. **(C)** ELISA for pERK/ERK showed a 4-fold increase in pERK/ERK of *dNf1* mutants compared to WT flies. Error bars indicate the standard deviation between duplicate samples. A paired, two-tailed t-test was performed to determine significance; *P < 0.05. **(D)** In RNAi Nf1 mutant flies, CQ significantly reduced the survival time compared to CQ-treated RNAi control flies, and untreated flies. **(E)** CQ resulted in increased lethality of *dNf1*$^{C1}$/*dNf1*$^{C2}$ mutants compared to WT flies. We were able to rescue the sensitivity of *dNF1* mutant flies to CQ by re-expression of dNf1 from a *UAS-dNF1* transgene.

**Figure 8. Combined effect of Selumetinib with CQ, Bafilomycin A1, AZT, and Enzalutamide on cell viability.**

**(A)** *Drosophila* NF1 KO cells were treated with 0 μM or 10 μM Selumetinib combined with CQ. Alone, Selumetinib significantly reduced the viability of both WT and NF1 KO cells to the same extent. As noted previously, CQ alone significantly reduced the viability of NF1-KO cells compared to WT. However, in combination with CQ, Selumetinib resulted in a significantly greater reduction in NF1 KO cell viability compared to CQ alone, which was not observed in WT cells (*P<0.05 vs 0 μM Selumetinib and **P<0.01 vs WT).

## SUPPLEMENTAL INFORMATION

**Table S1. The genome-wide dsRNA screen identified 134 synthetic lethal partner genes to NF1**

**Table S2. Further screening of the 134 synthetic lethal partner genes identified 54 candidate genes with human orthologs**

**Table S3. Statistical enrichment analysis of the 54 candidate genes identified a further 22 candidate genes that were druggable targets.** Table 3a shows the GO enriched terms for the candidate gene list. Table 3b shows the semantic similarity analysis of candidate GO terms with NF1 GO terms (yellow: 0.6-0.8 “part of a relationship, red: >0.8 “in a relationship”). Table 3c shows the newly identified HITS from each analysis, with a final list of those that can be targeted with FDA-approved drugs.

**Fig. S1. The *NF1* gene is well conserved between *Drosophila* and humans with 68% identity at the amino acid level.**

**Fig. S2. Drug dose curves. (A)** Dose curves for the 15 drugs with *Drosophila* orthologs as targets in WT and NF1-KO S2R+ cells. **(B)** Dose curves for CQ and Bafilomycin A1 addition to dose curves with the two drugs without *Drosophila* ortholog targets (AZT and Enzalutamide) in human CRISPR/Cas9 genome edited Schwann cells ($NF1^{+/-}$ and $NF1^{-/-}$).

Figure 1

**A**

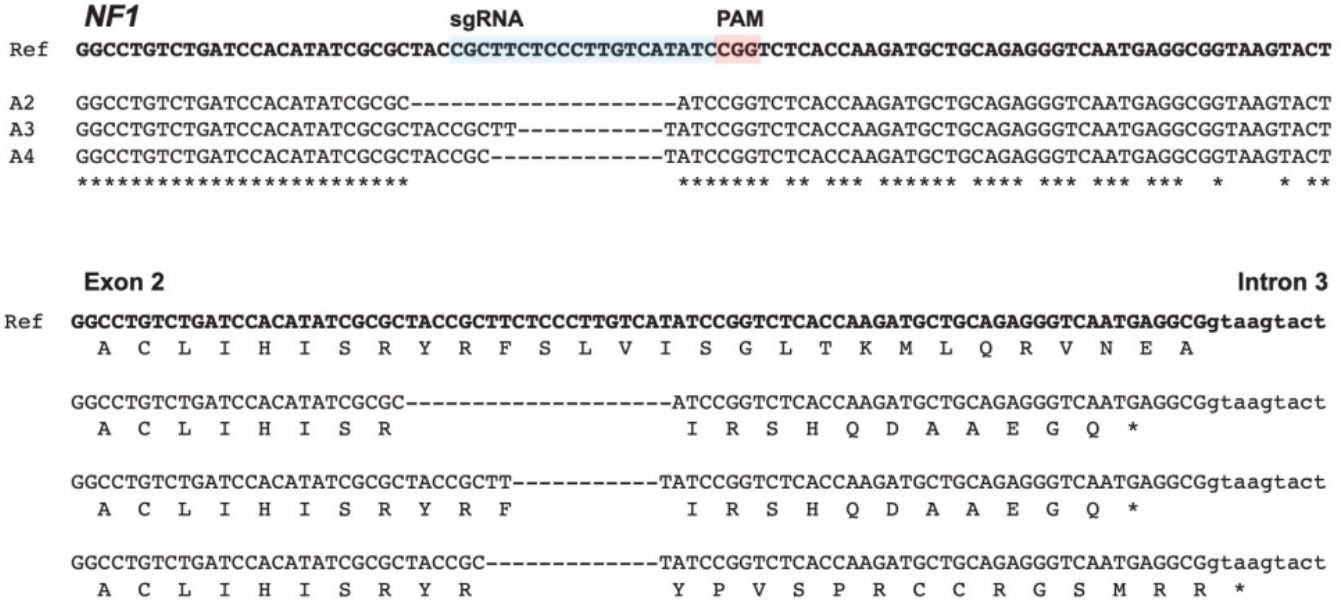
NF1
sgRNA
PAM
Ref GGCCTGTCTGATCCACATATCGCGCTACCGCTTCTCCCTTGTCATATCCGGTCTCACCAAGATGCTGCAGAGGGTCAATGAGGCGGTAAGTACT
A2 GGCCTGTCTGATCCACATATCGCGC----------ATCCGGTCTCACCAAGATGCTGCAGAGGGTCAATGAGGCGGTAAGTACT
A3 GGCCTGTCTGATCCACATATCGCGCTACCGCTT----------TATCCGGTCTCACCAAGATGCTGCAGAGGGTCAATGAGGCGGTAAGTACT
A4 GGCCTGTCTGATCCACATATCGCGCTACCGC----------TATCCGGTCTCACCAAGATGCTGCAGAGGGTCAATGAGGCGGTAAGTACT
Exon 2
Intron 3
Ref GGCCTGTCTGATCCACATATCGCGCTACCGCTTCTCCCTTGTCATATCCGGTCTCACCAAGATGCTGCAGAGGGTCAATGAGGCGgtaagtact
A C L I H I S R Y R F S L V I S G L T K M L Q R V N E A
GGCCTGTCTGATCCACATATCGCGC----------ATCCGGTCTCACCAAGATGCTGCAGAGGGTCAATGAGGCGgtaagtact
A C L I H I S R I R S H Q D A A E G Q *
GGCCTGTCTGATCCACATATCGCGCTACCGCTT----------TATCCGGTCTCACCAAGATGCTGCAGAGGGTCAATGAGGCGgtaagtact
A C L I H I S R Y R F I R S H Q D A A E G Q *
GGCCTGTCTGATCCACATATCGCGCTACCGC----------TATCCGGTCTCACCAAGATGCTGCAGAGGGTCAATGAGGCGgtaagtact
A C L I H I S R Y R Y P V S P R C C R G S M R R *

**B**

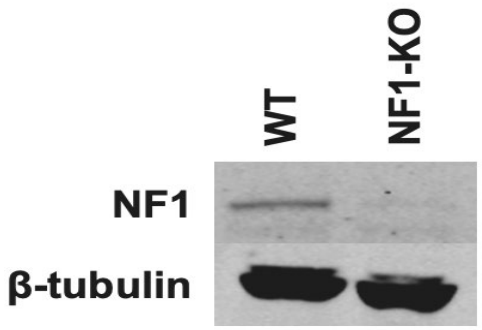
WT
NF1-KO
NF1
β-tubulin

**C**

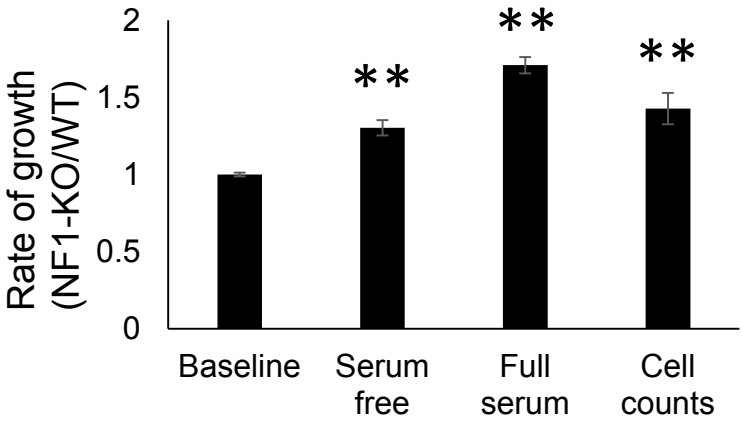
Rate of growth (NF1-KO/WT)
2
1.5
1
0.5
0
**
**
**
Baseline
Serum free
Full serum
Cell counts

Figure 2

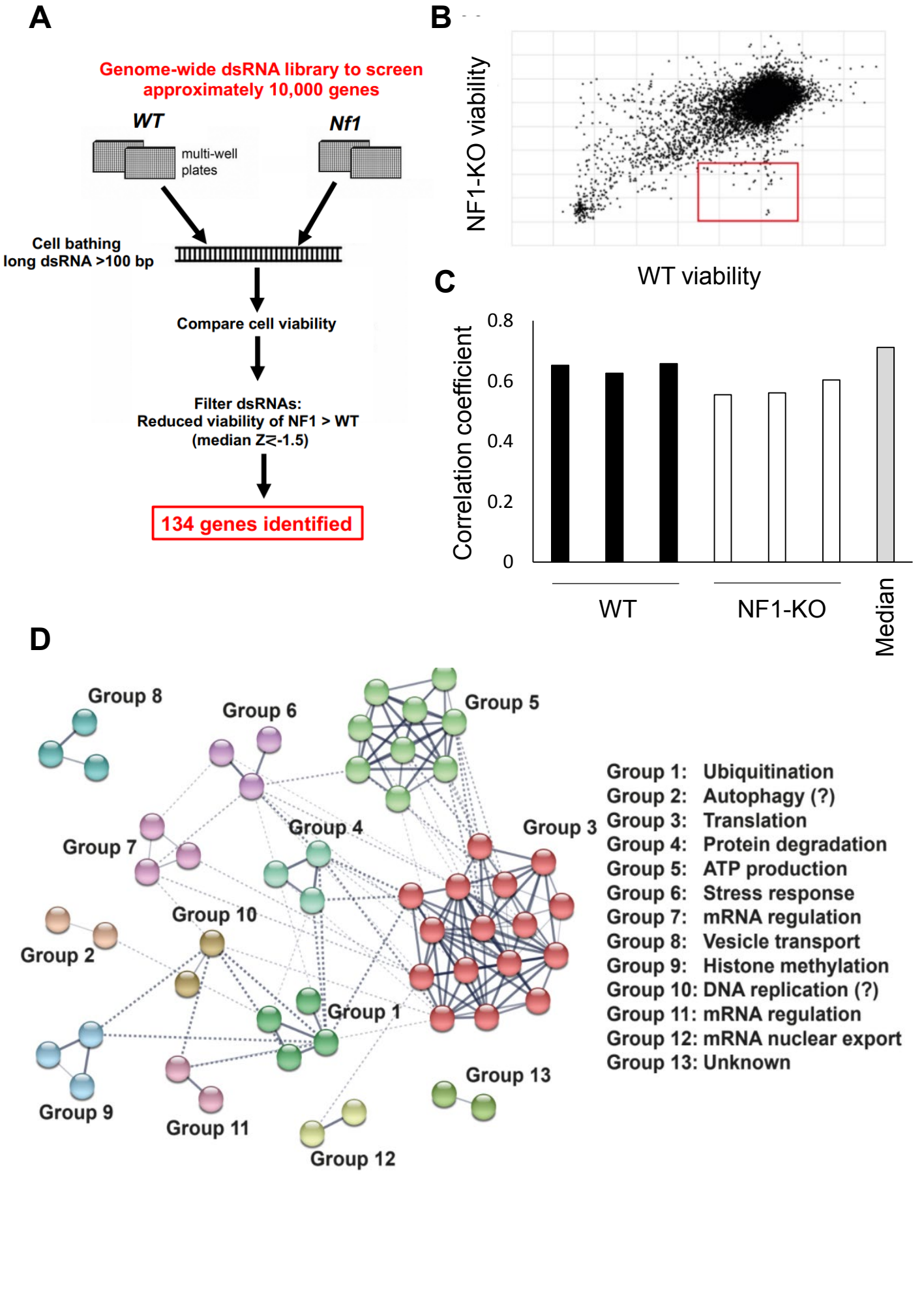
A
Genome-wide dsRNA library to screen approximately 10,000 genes
WT
Nf1
multi-well plates
Cell bathing long dsRNA >100 bp
Compare cell viability
Filter dsRNAs: Reduced viability of NF1 > WT (median Z≤-1.5)
134 genes identified
B
NF1-KO viability
WT viability
C
Correlation coefficient
0.8
0.6
0.4
0.2
0
WT
NF1-KO
Median
D
Group 8
Group 6
Group 5
Group 7
Group 4
Group 3
Group 10
Group 2
Group 1
Group 13
Group 9
Group 11
Group 12
Group 1: Ubiquitination
Group 2: Autophagy (?)
Group 3: Translation
Group 4: Protein degradation
Group 5: ATP production
Group 6: Stress response
Group 7: mRNA regulation
Group 8: Vesicle transport
Group 9: Histone methylation
Group 10: DNA replication (?)
Group 11: mRNA regulation
Group 12: mRNA nuclear export
Group 13: Unknown

Figure 3

A

**GO term enrichment**
- BP (215 terms)
- MF (43 terms)
- CC (79 terms)

**Semantic similarity analysis of GO terms (HIT and NF1) to identify drug targets**
e.g. *histone methyltransferase activity (H3-K4 specific)* and *N-methyltransferase activity*

**Additional FDA approved drug targets:**
*RAC1, EGFR, FGFR, EZH2, hTERT*

**KEGG Enrichment – 15 pathways including:**
**Proteosome**
**Ubiquitin mediated proteolysis**
**Oxidative phosphorylation**

**Additional FDA approved drug targets:**
*MYC, AR, CUL1, mTOR*

**Protein-protein interaction mapping to identify drug targets**
e.g. interaction between SHF (screen HIT) and PDGFRA (FDA-approved drug target)

**Additional FDA approved drug targets:**
*PDGFRA, RAF1, MEK, KRAS, MT-CYB, BECN1, RP, GFAP, SKP1, USP14, SAMHD1, CDC37*

B

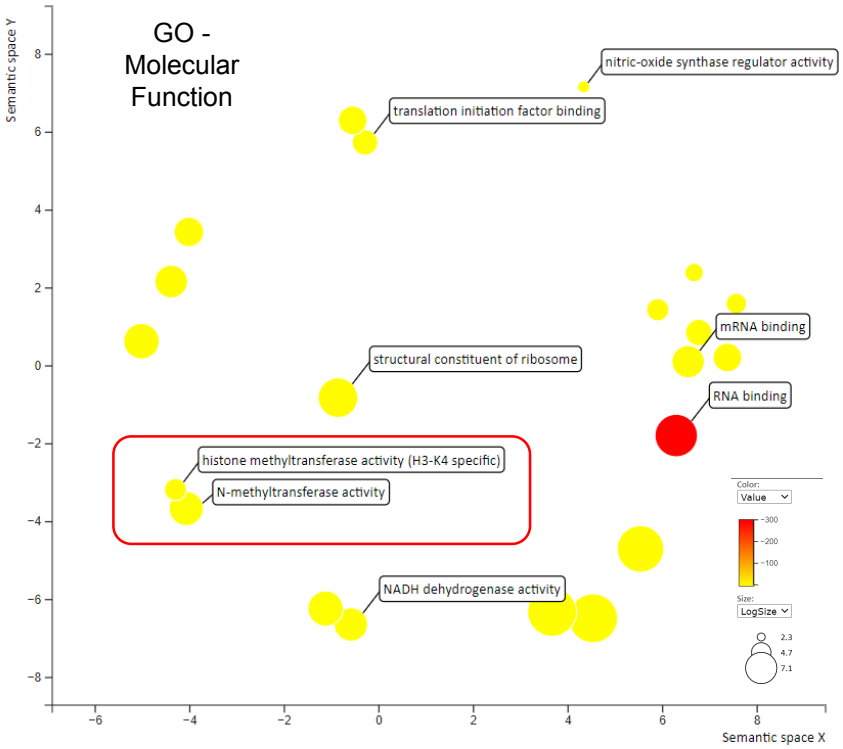


C KEGG pathway enrichment

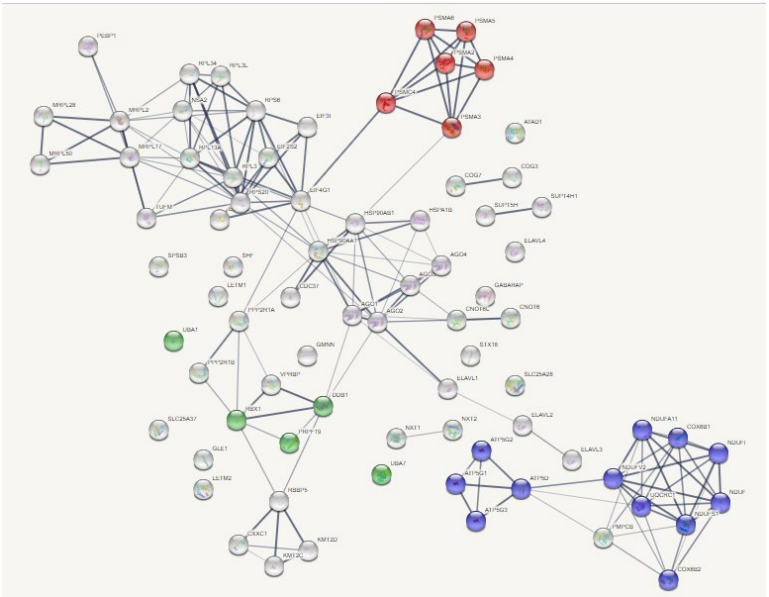

D Protein-protein interaction mapping:
*SHF - PDGFRA*

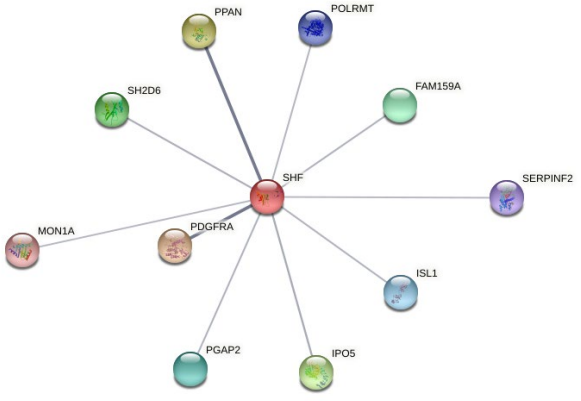

Figure 4

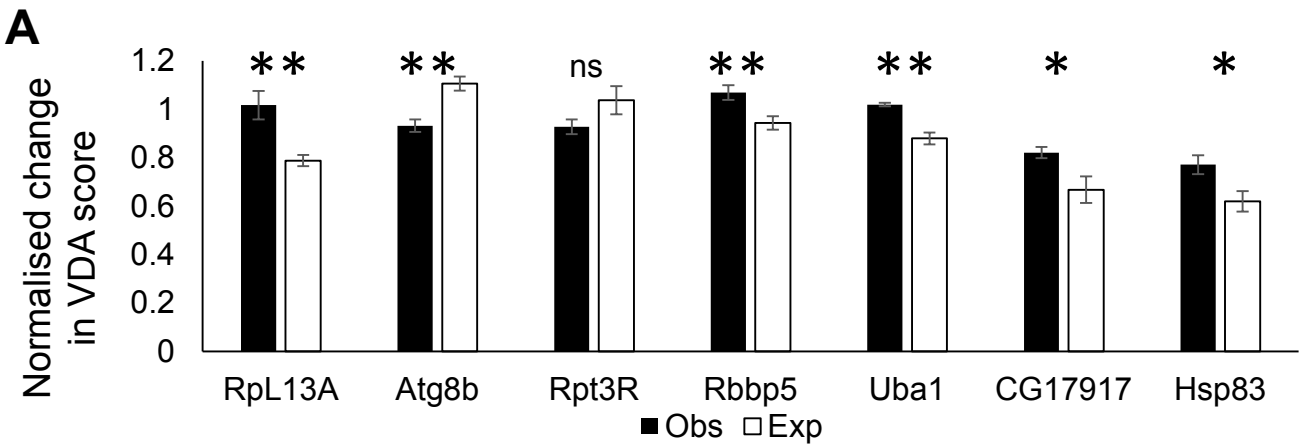
A
Normalised change in VDA score
1.2
1
0.8
0.6
0.4
0.2
0
**
**
ns
**
**
*
*
RpL13A
Atg8b
Rpt3R
Rbbp5
Uba1
CG17917
Hsp83
Obs
Exp

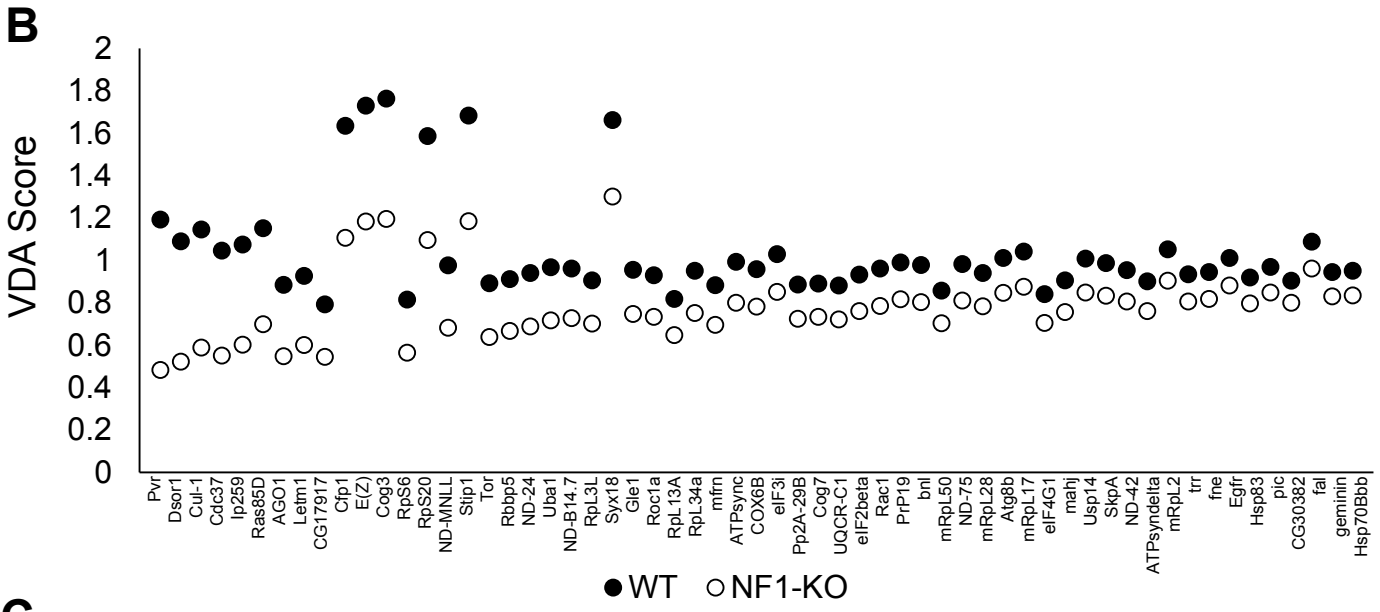
B
VDA Score
2
1.8
1.6
1.4
1.2
1
0.8
0.6
0.4
0.2
0
Pvr
Dsor1
Cul-1
Cdc37
Ip259
Ras85D
AGO1
Letm1
CG17917
Cfp1
E(Z)
Cog3
RpS6
RpS20
ND-MNLL
Stip1
Tor
Rbbp5
ND-24
Uba1
ND-B14.7
RpL3L
Syx18
Gle1
Roc1a
RpL13A
RpL34a
mfrn
ATPsync
COX6B
eIF3i
Pp2A-29B
Cog7
UQCR-C1
eIF2beta
Rac1
PrP19
bnl
mRpL50
ND-75
mRpL28
Atg8b
mRpL17
eIF4G1
mahj
Usp14
SkpA
ND-42
ATPsyndelta
mRpL2
trr
fne
Egfr
Hsp83
pic
CG30382
fal
geminin
Hsp70Bbb
WT
NF1-KO

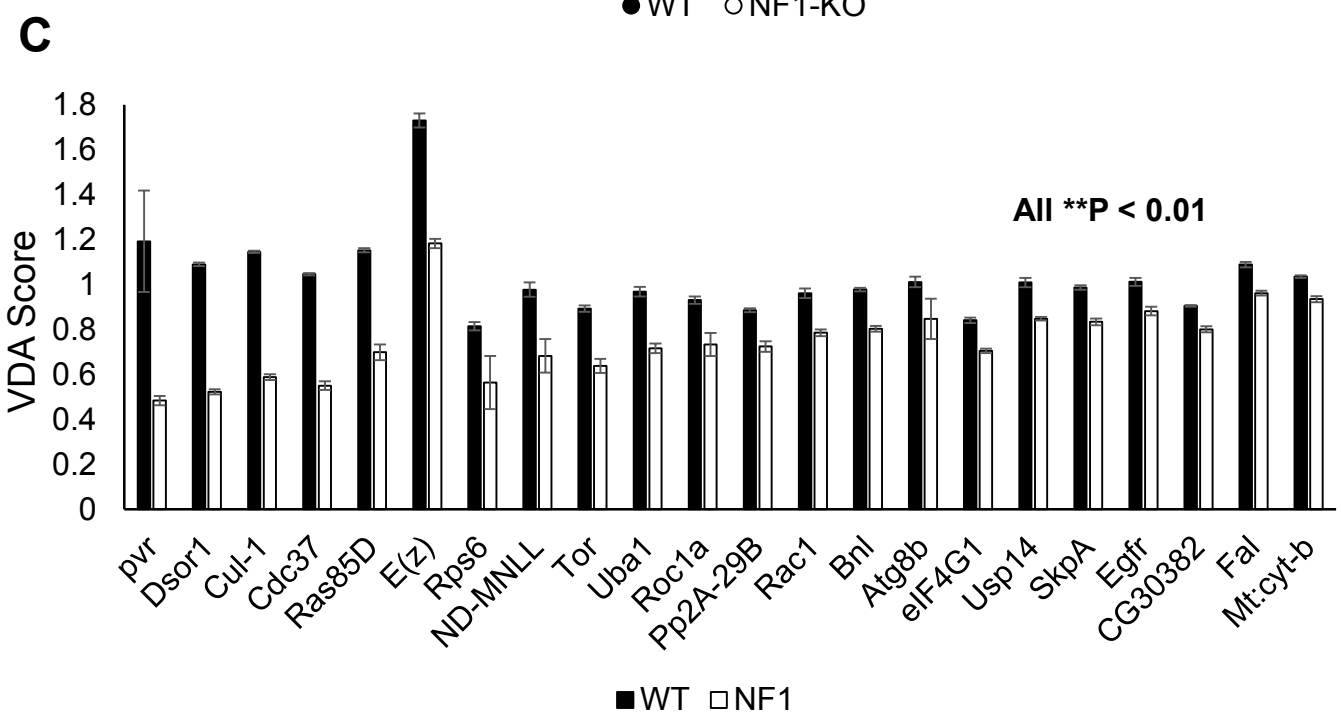
C
VDA Score
1.8
1.6
1.4
1.2
1
0.8
0.6
0.4
0.2
0
All **P < 0.01
pvr
Dsor1
Cul-1
Cdc37
Ras85D
E(z)
Rps6
ND-MNLL
Tor
Uba1
Roc1a
Pp2A-29B
Rac1
Bnl
Atg8b
eIF4G1
Usp14
SkpA
Egfr
CG30382
Fal
Mt:cyt-b
WT
NF1

Figure 5

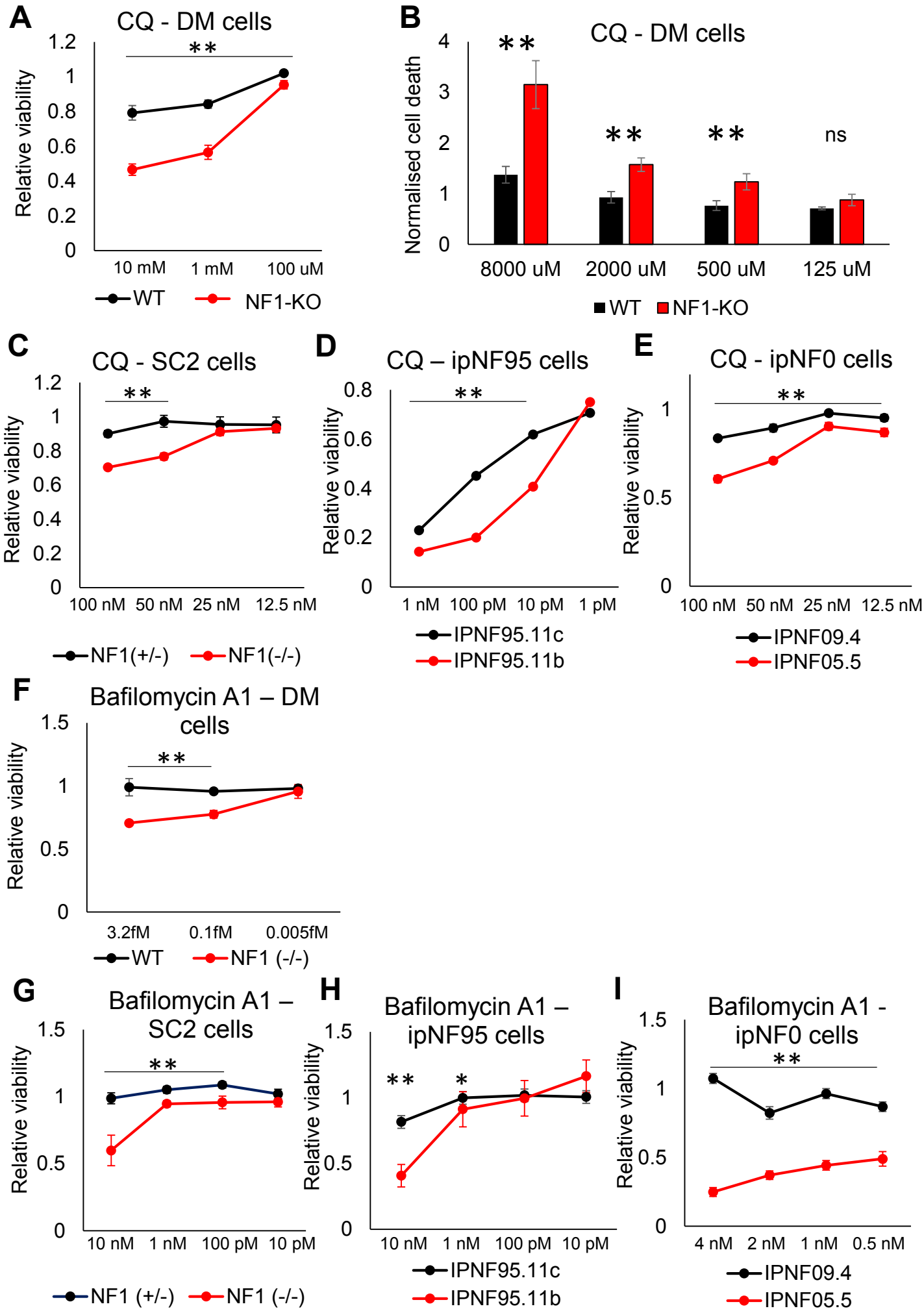
A
CQ - DM cells
Relative viability
1.2
1
0.8
0.6
0.4
0.2
0
**
10 mM
1 mM
100 uM
WT
NF1-KO
B
CQ - DM cells
Normalised cell death
4
3
2
1
0
**
**
**
ns
8000 uM
2000 uM
500 uM
125 uM
WT
NF1-KO
C
CQ - SC2 cells
Relative viability
1.2
1
0.8
0.6
0.4
0.2
0
**
100 nM
50 nM
25 nM
12.5 nM
NF1(+/-)
NF1(-/-)
D
CQ – ipNF95 cells
Relative viability
0.8
0.6
0.4
0.2
0
**
1 nM
100 pM
10 pM
1 pM
IPNF95.11c
IPNF95.11b
E
CQ - ipNF0 cells
Relative viability
1
0.5
0
**
100 nM
50 nM
25 nM
12.5 nM
IPNF09.4
IPNF05.5
F
Bafilomycin A1 – DM cells
Relative viability
1.5
1
0.5
0
**
3.2fM
0.1fM
0.005fM
WT
NF1 (-/-)
G
Bafilomycin A1 – SC2 cells
Relative viability
1.5
1
0.5
0
**
10 nM
1 nM
100 pM
10 pM
NF1 (+/-)
NF1 (-/-)
H
Bafilomycin A1 – ipNF95 cells
Relative viability
1.5
1
0.5
0
**
*
10 nM
1 nM
100 pM
10 pM
IPNF95.11c
IPNF95.11b
I
Bafilomycin A1 - ipNF0 cells
Relative viability
1.5
1
0.5
0
**
4 nM
2 nM
1 nM
0.5 nM
IPNF09.4
IPNF05.5

Figure 6

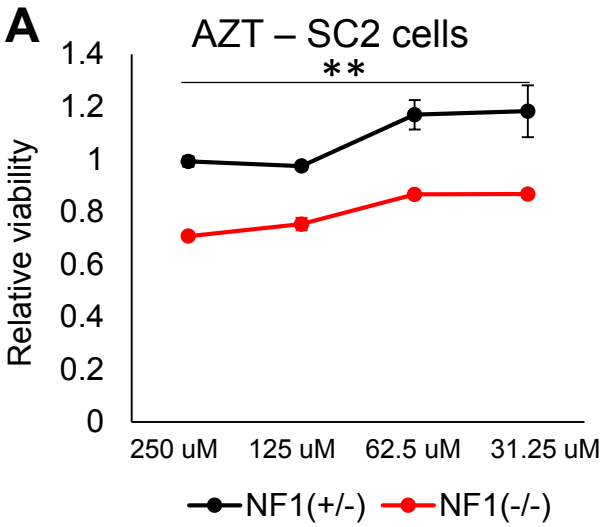
A
AZT – SC2 cells
**
Relative viability
1.4
1.2
1
0.8
0.6
0.4
0.2
0
250 uM
125 uM
62.5 uM
31.25 uM
NF1(+/-)
NF1(-/-)

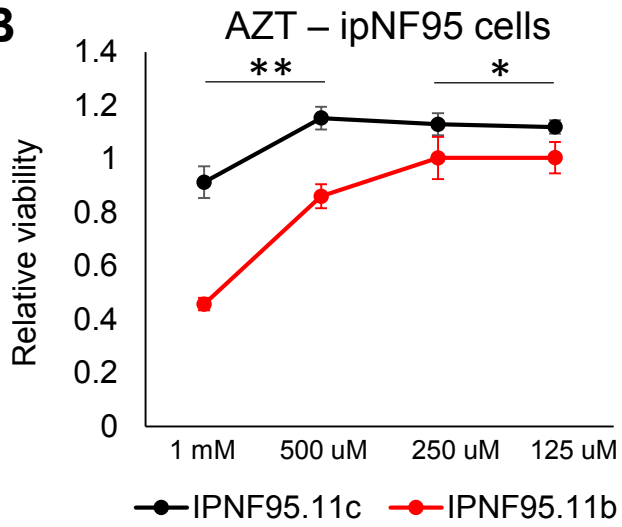
B
AZT – ipNF95 cells
**
*
Relative viability
1.4
1.2
1
0.8
0.6
0.4
0.2
0
1 mM
500 uM
250 uM
125 uM
IPNF95.11c
IPNF95.11b

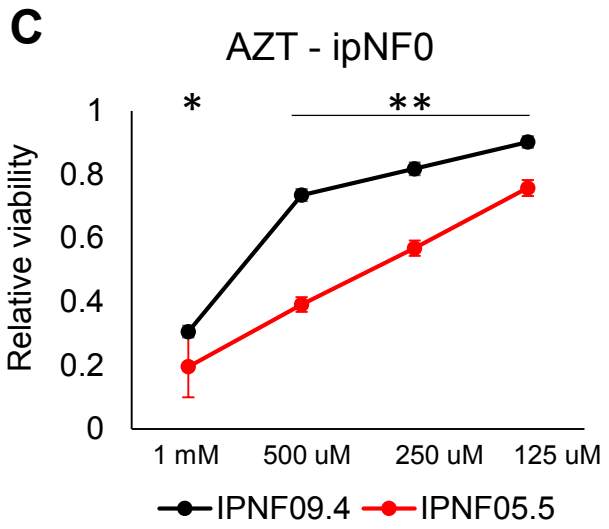
C
AZT - ipNF0
*
**
Relative viability
1
0.8
0.6
0.4
0.2
0
1 mM
500 uM
250 uM
125 uM
IPNF09.4
IPNF05.5

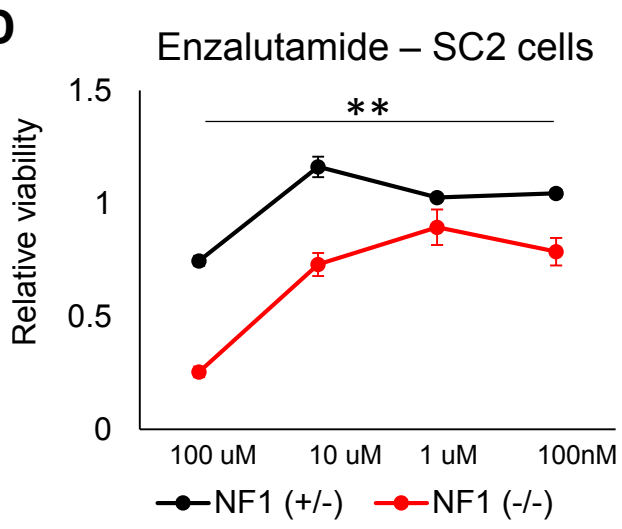
D
Enzalutamide – SC2 cells
**
Relative viability
1.5
1
0.5
0
100 uM
10 uM
1 uM
100nM
NF1 (+/-)
NF1 (-/-)

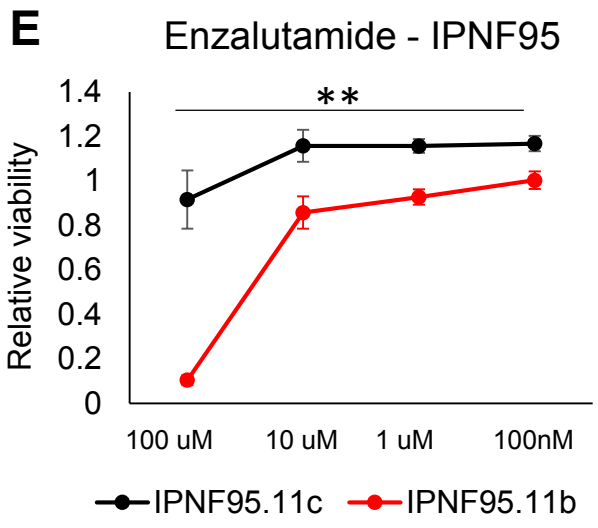
E
Enzalutamide - IPNF95
**
Relative viability
1.4
1.2
1
0.8
0.6
0.4
0.2
0
100 uM
10 uM
1 uM
100nM
IPNF95.11c
IPNF95.11b

Figure 7

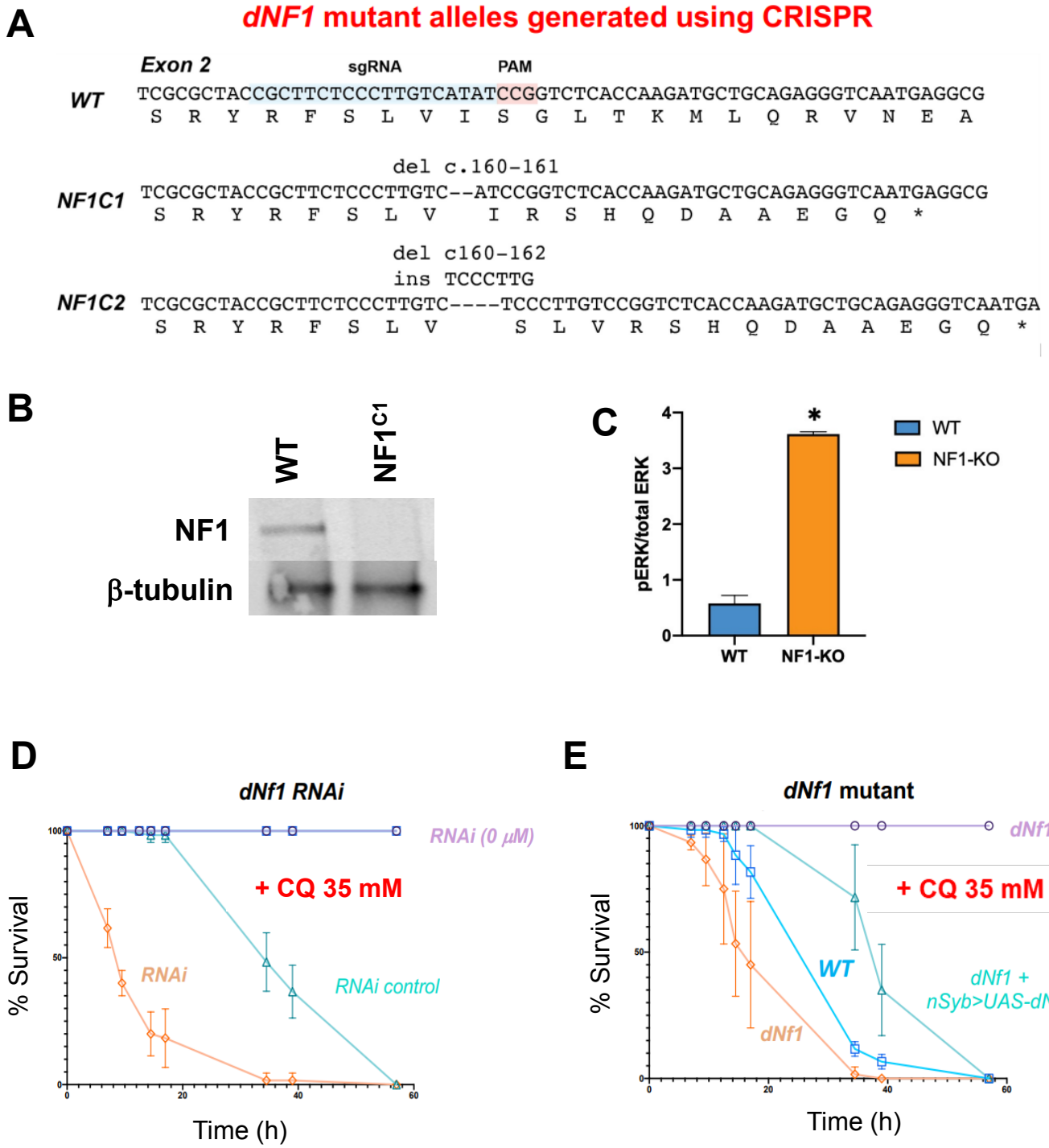
A
dNF1 mutant alleles generated using CRISPR
Exon 2
sgRNA
PAM
WT
TCGCGCTACCGCTTCTCCCTTGTCATATCCGGTCTCACCAAGATGCTGCAGAGGGTCAATGAGGCG
S R Y R F S L V I S G L T K M L Q R V N E A
del c.160-161
NF1C1
TCGCGCTACCGCTTCTCCCTTGTC--ATCCGGTCTCACCAAGATGCTGCAGAGGGTCAATGAGGCG
S R Y R F S L V I R S H Q D A A E G Q *
del c160-162
ins TCCCTTG
NF1C2
TCGCGCTACCGCTTCTCCCTTGTC----TCCCTTGTCCGGTCTCACCAAGATGCTGCAGAGGGTCAATGA
S R Y R F S L V S L V R S H Q D A A E G Q *
B
WT
NF1C1
NF1
β-tubulin
C
pERK/total ERK
WT
NF1-KO
*
D
dNf1 RNAi
RNAi (0 μM)
+ CQ 35 mM
RNAi
RNAi control
% Survival
Time (h)
E
dNf1 mutant
dNf1 (0 μM)
+ CQ 35 mM
WT
dNf1
dNf1 +
nSyb>UAS-dNF1
% Survival
Time (h)

Figure 8

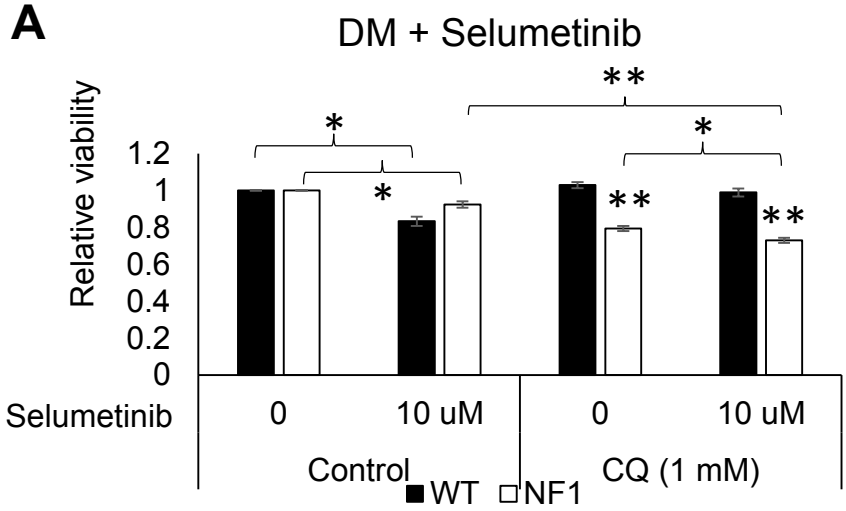
A
DM + Selumetinib
Relative viability
1.2
1
0.8
0.6
0.4
0.2
0
Selumetinib
0
10 uM
0
10 uM
Control
CQ (1 mM)
WT
NF1
*
*
*
**
**
**

# Fig. S1. The *NF1* gene is well conserved between *Drosophila* and humans with 68% identity at the amino acid level.

**Sequence 1:** NP_733132.2 **Gene:** Nf1 / 43149 **FlyBaseID:** FBgn0015269 **Length:** 2802 **Species:** Drosophila melanogaster
**Sequence 2:** NP_001035957.1 **Gene:** NF1 / 4763 **HGNCID:** 7765 **Length:** 2839 **Species:** Homo sapiens

**Alignment Length:** 2960 **Identity:** 1608/2961 (54%)
**Similarity:** 2026/2961 (68%) **Gaps:** 322/2961 (11%)

**Fig. S2. Drug dose curves. (A)** Dose curves for the 15 drugs with *Drosophila* orthologs as targets in WT and NF1-KO S2R+ cells. **(B)** Dose curves for CQ and Bafilomycin addition to dose curves with the two drugs without *Drosophila* ortholog targets (AZT and Enzalutamide) in human CRISPR/Cas9 genome edited Schwann cells ($NF1^{+/-}$ and $NF1^{-/-}$).

**A**

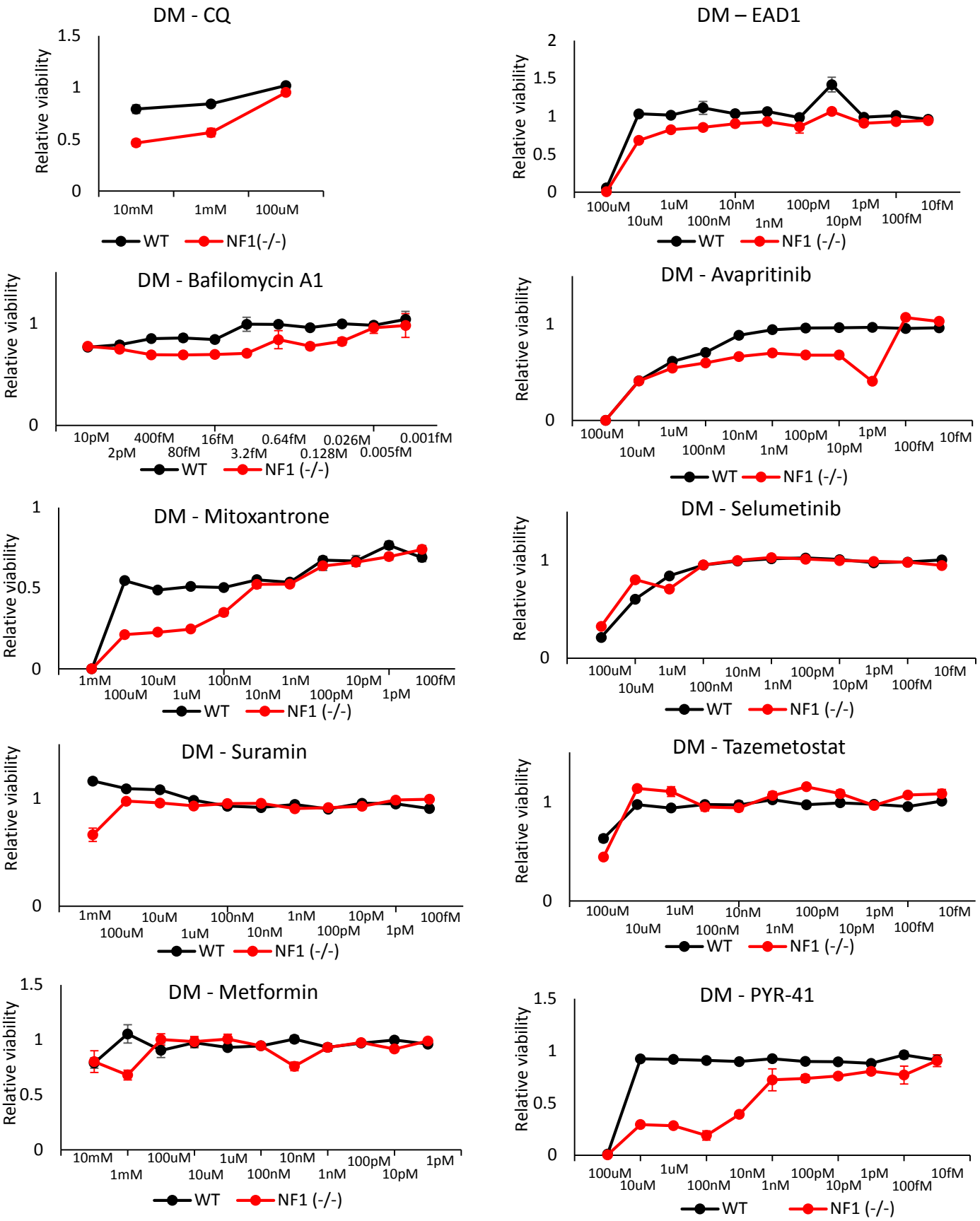

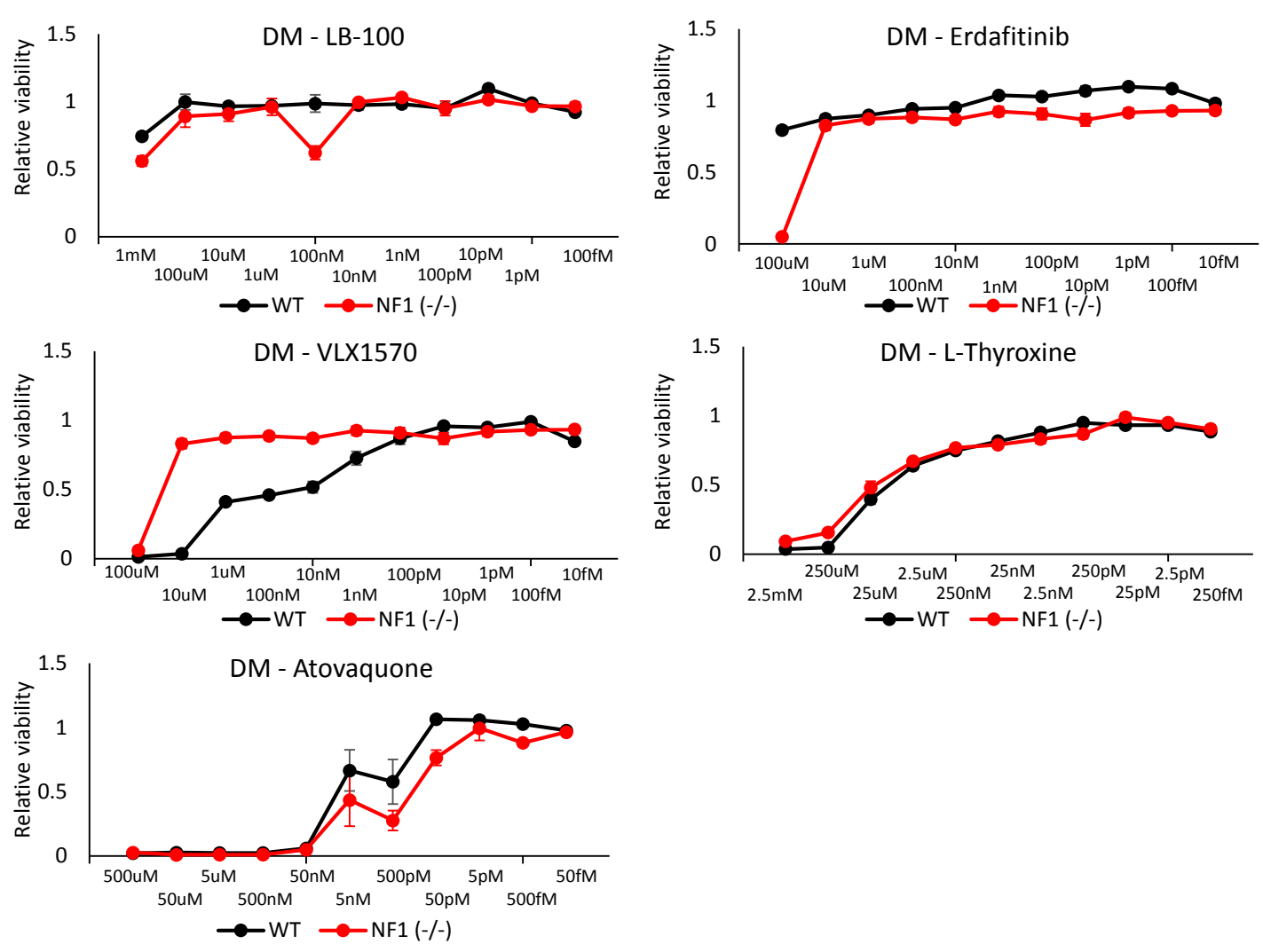
DM - LB-100
Relative viability
1.5
1
0.5
0
1mM
100uM
10uM
1uM
100nM
10nM
1nM
100pM
10pM
1pM
100fM
WT
NF1 (-/-)
DM - Erdafitinib
Relative viability
100uM
10uM
1uM
100nM
10nM
1nM
100pM
10pM
1pM
100fM
10fM
WT
NF1 (-/-)
DM - VLX1570
Relative viability
100uM
10uM
1uM
100nM
10nM
1nM
100pM
10pM
1pM
100fM
10fM
WT
NF1 (-/-)
DM - L-Thyroxine
Relative viability
2.5mM
250uM
25uM
2.5uM
250nM
25nM
2.5nM
250pM
25pM
2.5pM
250fM
WT
NF1 (-/-)
DM - Atovaquone
Relative viability
500uM
50uM
5uM
500nM
50nM
5nM
500pM
50pM
5pM
500fM
50fM
WT
NF1 (-/-)

**B**

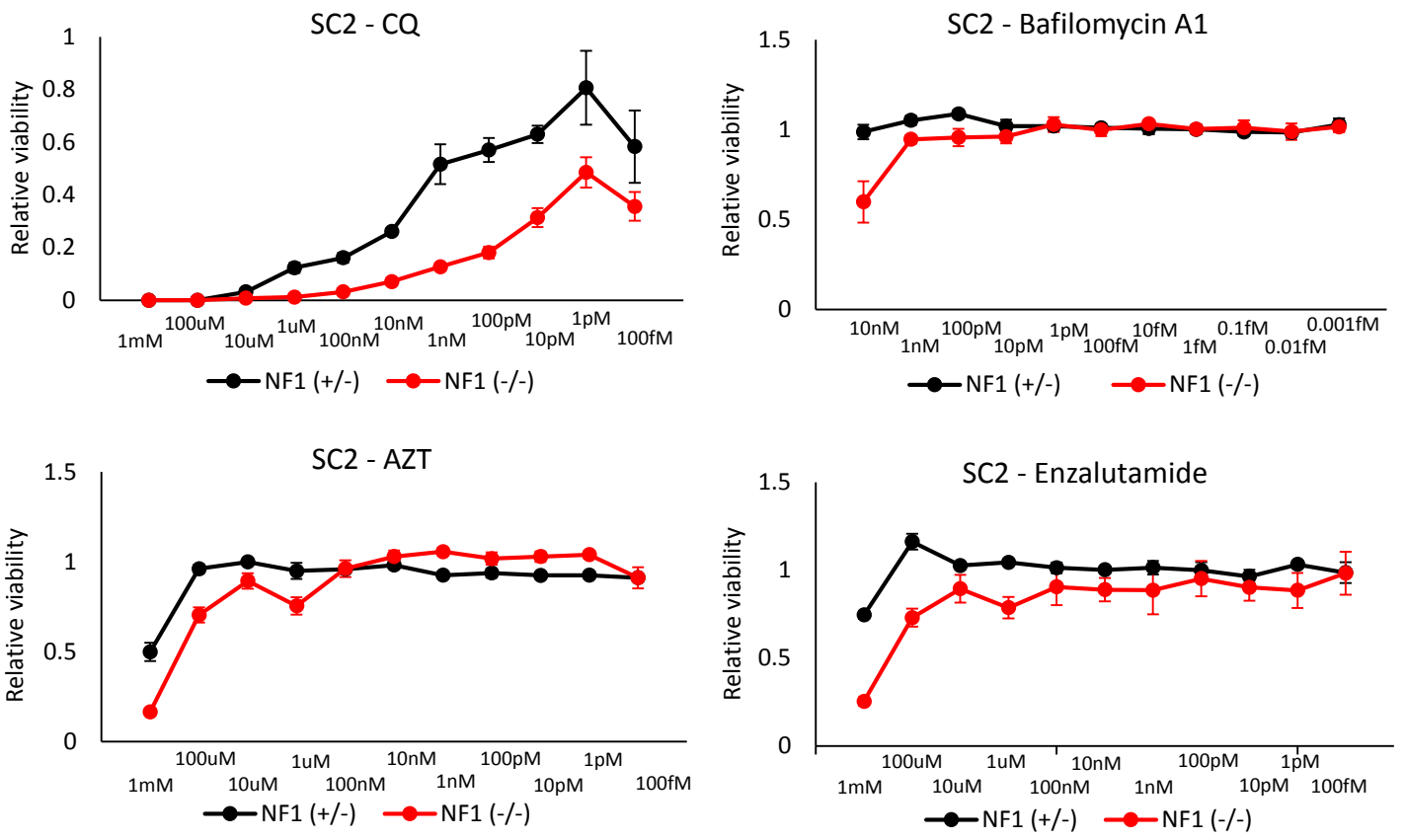
SC2 - CQ
Relative viability
1
0.8
0.6
0.4
0.2
0
1mM
100uM
10uM
1uM
100nM
10nM
1nM
100pM
10pM
1pM
100fM
NF1 (+/-)
NF1 (-/-)
SC2 - Bafilomycin A1
Relative viability
10nM
1nM
100pM
10pM
1pM
100fM
10fM
1fM
0.1fM
0.01fM
0.001fM
NF1 (+/-)
NF1 (-/-)
SC2 - AZT
Relative viability
1mM
100uM
10uM
1uM
100nM
10nM
1nM
100pM
10pM
1pM
100fM
NF1 (+/-)
NF1 (-/-)
SC2 - Enzalutamide
Relative viability
1mM
100uM
10uM
1uM
100nM
10nM
1nM
100pM
10pM
1pM
100fM
NF1 (+/-)
NF1 (-/-)